Available online at www.sciencedirect.com
SCIENCE DIRECT®
Journal of Computational Physics 192 (2003) 175–210
JOURNAL OF COMPUTATIONAL PHYSICS
www.elsevier.com/locate/jcp

Hybrid flux-splitting schemes for a common two-fluid model

Steinar Evje [a,*], Tore Flåtten [b]

[a] RF-Rogaland Research, Thormøhlensgt. 55, Bergen N-5008, Norway
[b] Department of Energy and Process Engineering, Norwegian University of Science and Technology, Kolbjørn Hejes vei 1B, Trondheim N-7491, Norway

Received 2 December 2002; received in revised form 10 July 2003; accepted 10 July 2003

Abstract

The aim of this paper is to construct hybrid flux vector splitting (FVS) and flux difference splitting (FDS) schemes for a commonly used two-fluid model consisting of two separate momentum equations. This is done by refining ideas previously applied to develop hybrid FVS/FDS schemes for a simpler two-phase model consisting of a mixture momentum equation [J. Comput. Phys. 175 (2002) 674]. More specifically, we seek to construct upwind type of schemes which are not based on calculations of the full eigenstructure of Jacobi matrices as needed by approximate Riemann solvers like the Roe scheme. Based on a crude approximation of the eigenstructure of the model, we derive schemes of the van Leer and FVS type. We demonstrate that these schemes possess desirable stability properties, but are excessively diffusive. By adapting ideas originally suggested by Wada and Liou [SIAM J. Sci. Comput. 18 (1997) 633] for the Euler equations, we suggest a mechanism for removing numerical dissipation. We present numerical simulations where we compare the performance of the resulting schemes with that of the Roe scheme, and by that shed light on the issues of accuracy, efficiency, and robustness of the proposed schemes. Particularly, we consider the classical water faucet problem as well as a stiff separation problem which locally involves transition from two-phase to single-phase flow. Results from these test cases show that we are able to construct hybrid FVS/FDS schemes which properly combine the accuracy of FDS in the resolution of sharp mass fronts and the robustness of FVS which ensures stability under stiff conditions.

AMS: 76T10; 76N10; 65M12; 35L65

Keywords: Two-phase flow; Two-fluid model; Hyperbolic system of conservation laws; Flux vector splitting; Flux difference splitting; Hybrid scheme; Numerical dissipation

1. Introduction

Accurate resolution of the dynamics related to two-phase flow phenomena is of high importance, for instance, to the oil industry. Among several two-phase flow models there are two fundamentally different

* Corresponding author. Tel.: +47-55-54-38-50; fax: +47-55-54-38-60.
E-mail addresses: steinar.evje@rf.no (S. Evje), tore.flatten@maskin.ntnu.no (T. Flåtten).

0021-9991/$ - see front matter © 2003 Elsevier B.V. All rights reserved.
doi:10.1016/j.jcp.2003.07.001

formulations of the macroscopic field equations for the two-phase flow system; namely the *two-fluid* model and the *mixture* model [30]. Here we focus on the two-fluid model. This is considered to give the most general and detailed description of transient two-phase flows. In the two-fluid model each phase is treated separately in terms of two sets of conservation equations; one for each phase. The interaction terms between the two phases appear in the basic equations as transfer terms across the interfaces (source terms).

It seems that many authors agree on the basic form of the two-fluid model, see for instance [5]. However, due to the lack of some physical properties as well as the appearance of complex eigenvalues (loss of hyperbolicity), the derivation and inclusion of additional terms in the two-fluid model has been widely studied. In this work, we consider a common variant of the two-fluid model. Our main concern is to develop simple schemes whose numerical dissipation mechanism allows for producing stable and accurate predictions of two-phase flow phenomena relevant for the oil industry. A main issue is then accurate resolution of sharp mass fronts as well as stable and accurate calculations of flows where one of the two phases may disappear locally. More precisely, following [6], we have: If U denotes the vector of unknowns, the equations for the averaged two-fluid flow model are given by the system

$$\partial_t U + \partial_x f(U) + G(U)\partial_x U + \partial_x D(U, \partial_x U) = S(U).$$

Hence, the evolution of U is governed by convection, diffusion, and source terms. To a large extent the issue of accurate and stable approximation of typical mass transport problems is tightly connected to the convective part of the model, consequently, we focus on the first order variant of the above system given by

$$\partial_t U + \partial_x f(U) + G(U)\partial_x U = 0. \tag{1}$$

In particular, we do not discuss how to incorporate source terms and diffusion terms in the numerical schemes. However, an essential ingredient in the construction of numerical schemes for the two-fluid model, from our point of view, is that they should naturally allow for incorporation of more terms without changing the basic solution method. In this respect, we follow along the same line as Coquel et al. [5]. Another important aspect is that the numerical algorithms we study naturally can be used together with more complex equation of states (EOS).

Due to the wide range of fundamental and industrial applications of the two-fluid models, there has been a long-time interest in the development of efficient numerical algorithms for solving these models. The first computer models like CATHARE [2] were originally used to describe steam and water flow in nuclear reactors. It was based on pure advective upwinding, using a staggered grid together with implicit time integration to achieve stability. This approach was later adopted by the oil industry, resulting in computer codes like OLGA [3] and the more recently developed Petra [14]. These schemes are known to be robust, but diffusive and front-tracking methods have been incorporated to accurately resolve liquid slugs. In addition, they are not considered as being well suited for complex geometries.

During the last decade, various upwind type of schemes have been proposed for solving two-phase flow models, mixture models as well as two-fluid models. Many of these schemes, often categorized as flux difference splitting (FDS) schemes, are based on suitable modifications of classical upwind schemes like Godunov-type schemes [12,22] and Roe-type schemes [25,26]. Such schemes are accurate and robust, however they tend to be time consuming due to the need for repeated calculation of the Jacobian of the system with respect to the conservative variables. Examples of such upwind schemes for two-phase flow models include implementations of the Roe scheme by Toumi et al. [6,32,33], Romate [27], Tiselj and Petelin [31], Fjelde and Karlsen [11]. A rough Godunov scheme was implemented by Masella et al. [19]. Coquel et al. [5] studied kinetic upwind schemes, which do not make use of the eigenstructure, for the approximation of a general two-fluid model. They also demonstrated that these schemes could handle phase separation where fronts propagate and one of the two phases disappears locally.

Simpler schemes of the FVS type are based on dividing the numerical flux function $\mathbf{F}$ into positive and negative parts

$$\mathbf{F}(\mathbf{U}) = \mathbf{F}^-(\mathbf{U}) + \mathbf{F}^+(\mathbf{U}).$$

The numerical flux at the cell interface $j + 1/2$ is now given as

$$\mathbf{F}_{j+1/2}(\mathbf{U}_j, \mathbf{U}_{j+1}) = \mathbf{F}^+(\mathbf{U}_j) + \mathbf{F}^-(\mathbf{U}_{j+1}). \tag{2}$$

FDS is based on matrix calculations, while FVS is based on scalar calculations. Consequently, FVS is more efficient than FDS, however at the price of introducing excessive numerical dissipation. During the last years, a lot of research has been done for the Euler equations motivated by the desire to combine the efficiency of FVS and the accuracy of FDS. These schemes are not FVS anymore, since their numerical flux typically no longer can be expressed in the splitting form (2). They are a hybrid of FVS and FDS. We refer to the works of Liou et al. [7,17,18,35] for more background on these methods, commonly denoted as Advection Upstream Splitting Methods (AUSM).

Recently, some of these ideas have been adapted to two-phase flow models. Here, we mention the works of Niu [20] and Edwards et al. [8]. Niu explored hybrid flux-type flux splitting schemes for a multicomponent flow model, whereas Edwards et al. studied a homogeneous equilibrium two-phase model with phase transitions. Characteristic for these models is that they are very similar to the Euler systems in structure and mathematical character. Evje and Fjelde [9,10] considered a simplified isothermal two-phase model consisting of separate mass conservation equations and a mixture momentum equation. This model is more difficult to solve, since no analytical expression for the Jacobian is available. This is due to the fact that the model has to be supplemented with a more or less complicated slip relation leading to unequal fluid velocities. In [9,10] a rough estimate of the sound velocity of the two-phase model was employed in the construction of hybrid FVS/FDS schemes. Basically, it was found that the corresponding rough AUSM scheme was suitable for simulating typical mass transport flow cases relevant for the oil industry. The scheme gave accurate and non-oscillatory resolution of mass fronts (comparable with Roe scheme), also for flows where more general slip relations were used. In particular, it was demonstrated that the AUSM scheme possesses a positivity-preserving property which ensures that it is well suited for handling the case where one of the two phases may disappear locally. It was also observed that by introducing a hybrid FVS/FDS scheme denoted as AUSMV, which combines AUSM and FVS in an appropriate way, we obtained results comparable with the Roe scheme in the resolution of rapid pressure waves generated by this two-phase model.

In this paper, we consider a two-fluid model which possesses one momentum conservation equation for each phase. The model represents added complications in several ways.

- Motions of the two phases are no longer coupled in the same way as for the drift-flux model considered in [9,10] leading to flows with highly unequal phasic velocities.
- The two-fluid model involves non-conservative terms (the term $G(U)\partial_x U$ in (1)) which must be handled in a consistent manner by the numerical discretization.
- The two slowest eigenvalues are approximately equal and the model is very close to being parabolic. Indeed, additional terms must be added to the model to maintain hyperbolicity, i.e., avoid complex eigenvalues.

An extension of the AUSM$^+$ scheme for the Euler equations [17] was investigated by Paillère et al. [23] for this model. They based their approach on treating the model basically as two separate Euler models coupled through the pressure. They demonstrated that by including a pressure diffusion term, they were able to obtain stable and accurate solutions to several mass transport problems involving a local transition from two-phase to single-phase flow.

In the present work, we follow the approach of [9,10] and base the hybrid FVS/FDS schemes on a crude approximation of the eigenstructure of the model. First, we derive schemes of the van Leer and FVS type.

We demonstrate that these schemes possess desirable stability properties, but are excessively diffusive. By adapting ideas originally suggested by Wada and Liou [35] for the Euler equations, we suggest a mechanism for removing numerical dissipation. This leads to hybrid FVS/FDS schemes which will be denoted as AUSMV and AUSMD, which is in accordance with the notation used in [9,35]. In particular, we demonstrate:

- The AUSMD scheme is comparable with the Roe scheme for the classical water faucet problem [24] with respect to accuracy in the resolution of the discontinuity of the gas volume fraction. The AUSMV scheme is more diffusive than AUSMD.
- By introducing a slight modification of AUSMV, which ensures that the corresponding numerical flux coincides with that of the FVS scheme locally in the transition zone where the flow changes from two-phase to single-phase, this scheme produces stable and non-oscillatory solutions for the stiff separation problem considered in [5]. The AUSMD scheme is much less diffusive than AUSMV in the approximation of sharp mass fronts. This motivates us to construct a hybrid of AUSMV and AUSMD, denoted as AUSMDV, which produces excellent results for this stiff test case, when it is compared with an approximate analytical solution. The Roe scheme is not able to produce stable solutions for this problem due to the change from two-phase to single-phase flow.
- The hybrid FVS/FDS schemes presented here do not give non-oscillatory approximations of all waves for typical shock tube problems. However, it is observed that AUSMV converges to the same solution as the Roe scheme as the discretization parameters are taken to zero.

In view of the applications we have in mind, the important observation made in this work is that AUSMV/D give non-oscillatory, stable, and accurate approximations for typical mass transport problems, even when transition from two-phase to single-phase flow appears locally.

Finally, we would like to mention that Saurel and Abgrall [28] have suggested a non-conservative, unconditionally hyperbolic two-fluid model. Their model involves a separate pressure for each phase and an additional differential equation for the evolution of the volume fraction. A hybrid FVS/FDS scheme for this model has also been proposed by Niu [21].

Our paper is organized as follows: In Section 2, we present the two-fluid model that forms the basis for this work. In Section 3, we discuss some mathematical properties of this model and describe an implementation of a Roe scheme. The various flux-splitting schemes are introduced in Section 4. First, we briefly describe a van Leer scheme and an FVS scheme for the current two-fluid model. In particular, we describe a discretization of the non-conservative term that is consistent with how our Roe scheme treats this term. Then, we describe how to remove numerical dissipation from the van Leer and the FVS scheme, giving rise to two hybrid FVS/FDS type of schemes denoted as AUSMD and AUSMV, respectively. Section 5 is devoted to numerical experiments whose purpose is to highlight the stability and accuracy properties of the various schemes as observed when they are tested on several well-known flow cases.

2. The two-fluid model

The model we will be concerned with is formulated by stating separate conservation equations for mass and momentum for the two fluids, which we will denote as a gas (g) and a liquid (l) phase. For simplicity, we will assume an isentropic model and no energy equation will be taken into account.

We let $\mathbf{U}$ be the vector of conserved variables

$$\mathbf{U} = \begin{bmatrix} \rho_g \alpha_g \\ \rho_l \alpha_l \\ \rho_g \alpha_g v_g \\ \rho_l \alpha_l v_l \end{bmatrix} = \begin{bmatrix} u_1 \\ u_2 \\ u_3 \\ u_4 \end{bmatrix}. \tag{3}$$

The system of equations is given by

- Conservation of mass

$$\frac{\partial}{\partial t}(\rho_g \alpha_g) + \frac{\partial}{\partial x}(\rho_g \alpha_g v_g) = 0, \tag{4}$$

$$\frac{\partial}{\partial t}(\rho_l \alpha_l) + \frac{\partial}{\partial x}(\rho_l \alpha_l v_l) = 0. \tag{5}$$

- Conservation of momentum

$$\frac{\partial}{\partial t}(\rho_g \alpha_g v_g) + \frac{\partial}{\partial x}\left(\rho_g \alpha_g v_g^2 + \left(p_g - p_g^i\right)\alpha_g\right) + \alpha_g \frac{\partial p_g^i}{\partial x} = Q_g, \tag{6}$$

$$\frac{\partial}{\partial t}(\rho_l \alpha_l v_l) + \frac{\partial}{\partial x}\left(\rho_l \alpha_l v_l^2 + \left(p_l - p_l^i\right)\alpha_l\right) + \alpha_l \frac{\partial p_l^i}{\partial x} = Q_l, \tag{7}$$

where for phase k the nomenclature is as follows: ρ_k is the density; p_k is the pressure; v_k is the velocity; α_k is the volume fraction; p_k^i is the pressure at the gas–liquid interface; and Q_k is the momentum sources (due to gravity, friction, etc.).

We here treat Q_k as a pure source term, assuming that it does not contain any differential operators. To close the system we use the basic relation

$$\alpha_l + \alpha_g = 1. \tag{8}$$

In addition, appropriate thermodynamical submodels must be specified.

2.1. Thermodynamic submodels

For phase k, we assume the simplified linear thermodynamic relations

$$\rho_k = \rho_{k,0} + \frac{p_k - p_{k,0}}{a_k^2}. \tag{9}$$

The compressibilities are constant, given by

$$\frac{\partial p_k}{\partial \rho_k} = a_k^2. \tag{10}$$

Throughout this work, for the liquid phase we use the parameters

$$p_{l,0} = 1 \text{ bar} = 10^5 \text{ Pa},$$
$$\rho_{l,0} = 1000 \text{ kg/m}^3,$$

and

$$a_l = 10^3 \text{ m/s}.$$

For the gas phase we set

$$p_{g,0} = 0,$$
$$\rho_{g,0} = 0,$$

and

$$a_{\mathrm{g}}^2 = 10^5 \ (\mathrm{m/s})^2.$$

This constitutes a rough model of the behavior of air and water.

2.2. Interface pressure modelling

The pressure corrections $p_k - p_k^{\mathrm{i}}$ represent effects such as hydrostatics or surface tension and can effect the low wavelength dynamics of the system. We recall the well-known fact that the simplest assumption of equal pressure, $p_{\mathrm{g}} = p_{\mathrm{l}}$ and $p_k = p_k^{\mathrm{i}}$, will lead to a non-hyperbolic model whose applicability is questionable [29,30].

For a description of some common pressure correction models, we refer to the work of Cortes et al. [6] and the references therein. For the purposes of this paper, we will assume the equality of the phasic pressures, $p = p_{\mathrm{g}} = p_{\mathrm{l}}$, as well as $p_{\mathrm{i}} = p_{\mathrm{g}}^{\mathrm{i}} = p_{\mathrm{l}}^{\mathrm{i}}$. In this respect we follow the footsteps of [6,23].

For the interface pressure p_{i}, we choose the simple model

$$\Delta p = p - p_{\mathrm{i}} = \delta \frac{\alpha_{\mathrm{g}}\alpha_{\mathrm{l}}\rho_{\mathrm{g}}\rho_{\mathrm{l}}}{\rho_{\mathrm{g}}\alpha_{\mathrm{l}} + \rho_{\mathrm{l}}\alpha_{\mathrm{g}}}(v_{\mathrm{g}} - v_{\mathrm{l}})^2, \tag{11}$$

using $\delta = 1.2$. This choice ensures that the system is hyperbolic if the relative velocity $v_{\mathrm{r}} = v_{\mathrm{g}} - v_{\mathrm{l}}$ does not approach the sound velocity of the mixture. This assertion will be justified in Section 3.1 to follow.

We remark that the expression (11) is based on mathematical considerations and has little physical justification. However, a similar approach for achieving hyperbolicity was used for the CATHARE code [4], see also [6]. Paillère et al. [23] also based their investigations on this approach. Consistency with these previous works is our main motivation for choosing the model (11). We emphasize that we believe that the numerical techniques outlined in this paper are extensible to handle more general pressure correction models.

The assumption of equal pressure $p = p_{\mathrm{g}} = p_{\mathrm{l}}$ allows us to write the volume fraction Eq. (8) in terms of the conserved variables as

$$\frac{u_1}{\rho_{\mathrm{g}}(p)} + \frac{u_2}{\rho_{\mathrm{l}}(p)} = 1, \tag{12}$$

yielding the relation $p = p(u_1, u_2)$.

3. Eigenstructure and an approximate Riemann solver

3.1. Eigenstructure of the model

Writing the system in quasilinear form

$$\frac{\partial \mathbf{U}}{\partial t} + \mathbf{A}(\mathbf{U})\frac{\partial \mathbf{U}}{\partial x} = \mathbf{Q}(\mathbf{U}), \tag{13}$$

the Jacobi matrix $\mathbf{A}$ can be found to be

$$\mathbf{A}(\mathbf{U}) = \begin{bmatrix} 0 & 0 & 1 & 0 \\ 0 & 0 & 0 & 1 \\ \kappa\left(\rho_{\mathrm{l}}\alpha_{\mathrm{g}} + \Delta p \alpha_{\mathrm{l}} \frac{\partial \rho_{\mathrm{l}}}{\partial p}\right) - v_{\mathrm{g}}^2 & \kappa\left(\rho_{\mathrm{g}}\alpha_{\mathrm{g}} - \Delta p \alpha_{\mathrm{g}} \frac{\partial \rho_{\mathrm{g}}}{\partial p}\right) & 2v_{\mathrm{g}} & 0 \\ \kappa\left(\rho_{\mathrm{l}}\alpha_{\mathrm{l}} - \Delta p \alpha_{\mathrm{l}} \frac{\partial \rho_{\mathrm{l}}}{\partial p}\right) & \kappa\left(\rho_{\mathrm{g}}\alpha_{\mathrm{l}} + \Delta p \alpha_{\mathrm{g}} \frac{\partial \rho_{\mathrm{g}}}{\partial p}\right) - v_{\mathrm{l}}^2 & 0 & 2v_{\mathrm{l}} \end{bmatrix}, \tag{14}$$

where

$$\kappa = \frac{1}{(\partial\rho_l/\partial p)\alpha_l\rho_g + (\partial\rho_g/\partial p)\alpha_g\rho_l}. \tag{15}$$

The eigenvalues of the matrix **A** are the roots of the polynomial equation

$$\left[\kappa\left(\rho_l\alpha_g + \Delta p\alpha_l\frac{\partial\rho_l}{\partial p}\right) - (\lambda - v_g)^2\right]\left[\kappa\left(\rho_g\alpha_l + \Delta p\alpha_g\frac{\partial\rho_g}{\partial p}\right) - (\lambda - v_l)^2\right] - \kappa^2\left(\rho_g\alpha_g - \Delta p\alpha_g\frac{\partial\rho_g}{\partial p}\right)\left(\rho_l\alpha_l - \Delta p\alpha_l\frac{\partial\rho_l}{\partial p}\right) = 0. \tag{16}$$

These eigenvalues correspond to the wave velocities of the four eigenmodes of the model.

3.1.1. A perturbation method

Solving Eq. (16) exactly leads to highly complicated expressions and is not a practical approach. Instead, we adopt a technique suggested by Toumi and Kumbaro [33], who obtained approximate eigenvalues for a two-fluid model with a virtual mass force term. In the following, we use this technique to derive approximate eigenvalues for the current model involving the interface pressure correction term (11).

We introduce the perturbation parameter ε given by

$$\varepsilon = \frac{v_g - v_l}{\hat{c}(1+k)}, \tag{17}$$

where k is defined as

$$k = \frac{\rho_g\alpha_l}{\rho_l\alpha_g},$$

and $\hat{c}$ is an approximate mixture sound velocity given by

$$\hat{c} = \sqrt{\frac{\rho_l\alpha_g + \rho_g\alpha_l}{(\partial\rho_g/\partial p)\rho_l\alpha_g + (\partial\rho_l/\partial p)\rho_g\alpha_l}} = \sqrt{(\rho_l\alpha_g + \rho_g\alpha_l)\kappa}. \tag{18}$$

We further write Δp as

$$\frac{\Delta p}{\rho_l}\frac{\partial\rho_g}{\partial p} = \mathscr{P}\varepsilon^2.$$

We also introduce the new variables

$$\tilde{\alpha} = \frac{\alpha_l}{\alpha_g}, \quad \mu = \frac{\partial\rho_l}{\partial p}\Big/\frac{\partial\rho_g}{\partial p}, \quad z = \kappa\rho_l\alpha_g.$$

In particular, by using (18) we obtain the relation

$$1 + k = \frac{\hat{c}^2}{z}. \tag{19}$$

The eigenvalue equation (16) can now be written as

$$\left[z(1 + \mu\tilde{\alpha}\mathscr{P}\varepsilon^2) - (\lambda - v_g)^2\right]\left[z(k + \mathscr{P}\varepsilon^2) - (\lambda - v_l)^2\right] - z^2(k - \tilde{\alpha}\mathscr{P}\varepsilon^2)(1 - \mu\mathscr{P}\varepsilon^2) = 0. \tag{20}$$

Writing the eigenvalue as

$$\lambda = v_l + a\hat{c}$$

and invoking (19) and (17) yields the two relations

$$\frac{(\lambda - v_l)^2}{z} = \frac{a^2\hat{c}^2}{z} = a^2(1+k),$$
$$\frac{(\lambda - v_g)^2}{z} = \frac{(\lambda - v_l - \varepsilon\hat{c})^2}{z} = \frac{\hat{c}^2}{z}\left(\frac{\lambda - v_l}{\hat{c}} - \varepsilon\right)^2 = (1+k)(a - \varepsilon(1+k))^2.$$

Combining these with (20) yields the following equation for a:

$$\left[1 + \mu\tilde{\alpha}\mathscr{P}\varepsilon^2 - (1+k)(a - \varepsilon(1+k))^2\right][k + \mathscr{P}\varepsilon^2 - (1+k)a^2] = (k - \tilde{\alpha}\mathscr{P}\varepsilon^2)(1 - \mu\mathscr{P}\varepsilon^2). \tag{21}$$

A power series expansion yields

$$a(\varepsilon, \mathscr{P}, k, \mu, \tilde{\alpha}) = \sum_n \beta_n(k, \mu, \tilde{\alpha}, \mathscr{P})\varepsilon^n. \tag{22}$$

Inserting (22) into (21) and solving for the coefficients β_n we obtain:
E1: Downstream pressure wave
- $\beta_0 = 1$,
- $\beta_1 = 1$,
- $\beta_2 = (3k/2) + ((k-\alpha)(1-\mu)/2(1+k)^2)\mathscr{P}$.

E2: Upstream pressure wave
- $\beta_0 = -1$,
- $\beta_1 = 1$,
- $\beta_2 = -(3k/2) - ((k-\alpha)(1-\mu)/2(1+k)^2)\mathscr{P}$.

E3: Downstream void wave
- $\beta_0 = 0$,
- $\beta_1 = k + g$,
- $\beta_2 = 0$.

E4: Upstream void wave
- $\beta_0 = 0$,
- $\beta_1 = k - g$,
- $\beta_2 = 0$,

where we have used the shorthand

$$g = \sqrt{\frac{(1+\mu k)(1+\tilde{\alpha})}{(1+k)^2}\mathscr{P} - k}. \tag{23}$$

3.1.2. Approximate eigenvalues

We write the eigenvalues corresponding to pressure waves as

$$\lambda^{\mathrm{p}} = \bar{v}^{\mathrm{p}} \pm c, \tag{24}$$

whereas the eigenvalues corresponding to volume fraction waves are written as

$$\lambda^{\mathrm{v}} = \bar{v}^{\mathrm{v}} \pm \gamma. \tag{25}$$

By the results in Section 3.1.1, we obtain the approximations

$$\bar{v}^{\mathrm{p}} = \frac{\rho_{\mathrm{g}}\alpha_{\mathrm{l}}v_{\mathrm{l}} + \rho_{\mathrm{l}}\alpha_{\mathrm{g}}v_{\mathrm{g}}}{\rho_{\mathrm{g}}\alpha_{\mathrm{l}} + \rho_{\mathrm{l}}\alpha_{\mathrm{g}}} + \hat{c}\mathcal{O}(\varepsilon^3), \tag{26}$$

$$\bar{v}^{\mathrm{v}} = \frac{\rho_{\mathrm{g}}\alpha_{\mathrm{l}}v_{\mathrm{g}} + \rho_{\mathrm{l}}\alpha_{\mathrm{g}}v_{\mathrm{l}}}{\rho_{\mathrm{g}}\alpha_{\mathrm{l}} + \rho_{\mathrm{l}}\alpha_{\mathrm{g}}} + \hat{c}\mathcal{O}(\varepsilon^3), \tag{27}$$

$$c = \hat{c}(1 + \mathcal{O}(\varepsilon^2)), \tag{28}$$

$$\gamma = \sqrt{\frac{\Delta p(\rho_{\mathrm{g}}\alpha_{\mathrm{l}} + \rho_{\mathrm{l}}\alpha_{\mathrm{g}}) - \rho_{\mathrm{l}}\rho_{\mathrm{g}}\alpha_{\mathrm{l}}\alpha_{\mathrm{g}}(v_{\mathrm{g}} - v_{\mathrm{l}})^2}{(\rho_{\mathrm{g}}\alpha_{\mathrm{l}} + \rho_{\mathrm{l}}\alpha_{\mathrm{g}})^2}} + \hat{c}\mathcal{O}(\varepsilon^3), \tag{29}$$

where $\hat{c}$ is given by (18).

From (28) we see that the use of $\hat{c}$ as an approximate sound velocity is justified, while (29) clearly demonstrates that a zero pressure correction ($\Delta p = 0$) will render the model non-hyperbolic with complex eigenvalues. Note that the expression (11) with $\delta = 1$ corresponds exactly to $\gamma = 0$. For $\delta > 1$ we obtain $\gamma > 0$, whereas for $\delta < 1$ the parameter γ becomes imaginary. We remark that the analysis does not guarantee hyperbolicity if the higher order terms in ε become significant, i.e., if $\varepsilon \approx 1$.

Remark 1. To zeroth order in ε, i.e., the limit $v_{\mathrm{g}} = v_{\mathrm{l}} = v$, we have that

$$\lambda^{\mathrm{p}} = v \pm \hat{c} \tag{30}$$

and

$$\lambda^{\mathrm{v}} = v, \tag{31}$$

where λ^{v} now becomes a degenerate eigenvalue. It can be shown that the characteristic field corresponding to λ^{v} has the properties of a linearly degenerate field as long as this limit holds. Consequently, the eigenstructure of the equations, in this limit, becomes similar to the structure of the Euler equations [16]. This approximation will form the basis for our extension of numerical schemes for the Euler equations to the current two-fluid model, as will be described in Section 4.

3.2. Treatment of non-conservative integrals

In this section, we deal with the mathematical difficulties associated with the non-conservative terms in the momentum equations in the form

$$\alpha_k \frac{\partial p_{\mathrm{i}}}{\partial x}. \tag{32}$$

Eqs. (6) and (7) are perfectly valid for smooth flows where the derivatives exist. However, in the presence of discontinuities the differential formulation breaks down and the equations must be replaced with corresponding integral equations. For conservative systems, the corresponding integrals are well defined, but this is unfortunately not the case for non-conservative systems.

In this paper, we treat this issue largely following the approach of Toumi and Kumbaro [33]. We consider a discontinuity separating two states $(\mathbf{U}^{\mathrm{L}}, \mathbf{U}^{\mathrm{R}})$, where $\alpha_k^{\mathrm{L}} \neq \alpha_k^{\mathrm{R}}$ and $p_{\mathrm{i}}^{\mathrm{L}} \neq p_{\mathrm{i}}^{\mathrm{R}}$. The integral of (32) across this discontinuity is

$$\int_{\mathbf{U}^{\mathrm{L}}}^{\mathbf{U}^{\mathrm{R}}} \alpha_k \frac{\partial p_{\mathrm{i}}}{\partial s}\, \mathrm{d}s, \tag{33}$$

where $s(\mathbf{U})$ is a path linking the states $\mathbf{U}^{\mathrm{L}}$ and $\mathbf{U}^{\mathrm{R}}$. This integral is path-dependent and additional physical assumptions must be made to single out a unique path that will define the "correct" mathematical solution.

Toumi and Kumbaro [33] suggested writing (33) as

$$\int_{\mathbf{U}^{\mathrm{L}}}^{\mathbf{U}^{\mathrm{R}}} \alpha_k \frac{\partial p_{\mathrm{i}}}{\partial s}\, \mathrm{d}s = \bar{\alpha}\left(\alpha_k^{\mathrm{L}}, \alpha_k^{\mathrm{R}}\right)\left(p_{\mathrm{i}}^{\mathrm{R}} - p_{\mathrm{i}}^{\mathrm{L}}\right), \tag{34}$$

defining the path s indirectly through the choice of an averaging function $\bar{\alpha}(\alpha_k^{\mathrm{L}}, \alpha_k^{\mathrm{R}})$. In the case of incompressible liquid phase, they derived the harmonic average

$$\bar{\alpha}_{\mathrm{l}}\left(\alpha_{\mathrm{l}}^{\mathrm{L}}, \alpha_{\mathrm{l}}^{\mathrm{R}}\right) = \frac{2\alpha_{\mathrm{l}}^{\mathrm{L}}\alpha_{\mathrm{l}}^{\mathrm{R}}}{\alpha_{\mathrm{l}}^{\mathrm{L}} + \alpha_{\mathrm{l}}^{\mathrm{R}}} \tag{35}$$

by showing that the resulting non-conservative system has an equivalent conservative formulation.

Unfortunately this result relies heavily on the non-compressibility of the liquid phase and is not valid for the more general case where both phases are compressible. With no a priori difference between the gas and liquid phase, the basic equations (4)–(7) are symmetric under the interchange of phase labels. Hence, we insist that the averaging function $\bar{\alpha}(\alpha_k^{\mathrm{L}}, \alpha_k^{\mathrm{R}})$ must possess the same kind of phasic symmetry, which we express as

$$\bar{\alpha}\left(\alpha_k^{\mathrm{L}}, \alpha_k^{\mathrm{R}}\right) = 1 - \bar{\alpha}\left(1 - \alpha_k^{\mathrm{L}}, 1 - \alpha_k^{\mathrm{R}}\right). \tag{36}$$

Note that the harmonic average (35) does *not* satisfy the requirement (36). The arithmetic average, however, does satisfy (36). Consequently, for the purposes of this paper, we propose to use the averaging function

$$\bar{\alpha}\left(\alpha_k^{\mathrm{L}}, \alpha_k^{\mathrm{R}}\right) = \frac{1}{2}\left(\alpha_k^{\mathrm{L}} + \alpha_k^{\mathrm{R}}\right) \tag{37}$$

to define the non-conservative integrals of the form (34).

We emphasize that this choice is only one of many that satisfy the symmetry requirement (36). Here, we do not wish to advocate a particular strategy for dealing with the non-conservative term. Our concern is to ensure that the numerical schemes we investigate are mutually consistent in their treatment of the non-conservative integrals, making sure that the same momentum change is induced by a discontinuity in pressure and volume fraction. We stress that the hybrid flux-splitting schemes we developed in Section 4 are derived without making any assumptions of the particular functional form of $\bar{\alpha}(\alpha_k^{\mathrm{L}}, \alpha_k^{\mathrm{R}})$ and are trivially extensible to other choices of averaging functions.

3.3. Derivation of an approximate linearized Riemann solver

We are now in a position to derive a Roe scheme in the weak sense of Toumi and Kumbaro [33], where the Roe matrix $\hat{\mathbf{A}}$ satisfies the following conditions:

R1: $\hat{\mathbf{A}}(\mathbf{U}_1, \mathbf{U}_2)(\mathbf{U}_2 - \mathbf{U}_1) = \Delta\mathbf{F}(\mathbf{U}_1, \mathbf{U}_2)$,

R2: $\hat{\mathbf{A}}(\mathbf{U}_1, \mathbf{U}_2)$ is diagonalizable with real eigenvalues,

R3: $\hat{\mathbf{A}}(\mathbf{U}_1, \mathbf{U}_2) \to \mathbf{A}(\mathbf{U})$ smoothly as $\mathbf{U}_1, \mathbf{U}_2 \to \mathbf{U}$.

Here

$$\Delta\mathbf{F}(\mathbf{U}_1, \mathbf{U}_2) = \begin{bmatrix} \{\rho_{\mathrm{g}}\alpha_{\mathrm{g}}v_{\mathrm{g}}\} \\ \{\rho_{\mathrm{l}}\alpha_{\mathrm{l}}v_{\mathrm{l}}\} \\ \left\{\rho_{\mathrm{g}}\alpha_{\mathrm{g}}v_{\mathrm{g}}^2\right\} + \{\alpha_{\mathrm{g}}\Delta p\} + \bar{\alpha}_{\mathrm{g}}\{p - \Delta p\} \\ \left\{\rho_{\mathrm{l}}\alpha_{\mathrm{l}}v_{\mathrm{l}}^2\right\} + \{\alpha_{\mathrm{l}}\Delta p\} + \bar{\alpha}_{\mathrm{l}}\{p - \Delta p\} \end{bmatrix} \tag{38}$$

and $\{\cdot\}$ denotes the operation

$$\{x\} = x_2 - x_1.$$

Moreover, $\bar{\alpha}$ is given by (37) and $\mathbf{A}$ is the Jacobi matrix (14).

We now wish to obtain an average state $\widehat{\mathbf{U}}(\mathbf{U_1}, \mathbf{U_2})$ having the property that $\hat{\mathbf{A}}(\mathbf{U}_1, \mathbf{U}_2) = \mathbf{A}(\widehat{\mathbf{U}})$ satisfies the conditions R1–R3. The condition R1 gives rise to a set of coupled algebraic equations for $\widehat{\mathbf{U}}$ which may be solved to yield the result

$$\widehat{v} = \frac{v_1\sqrt{(\rho\alpha)_1} + v_2\sqrt{(\rho\alpha)_2}}{\sqrt{(\rho\alpha)_1} + \sqrt{(\rho\alpha)_2}},$$

$$\widehat{\alpha} = \frac{1}{2}(\alpha_1 + \alpha_2),$$

and

$$\widehat{\rho} = \frac{1}{2}(\rho_1 + \rho_2)$$

for each phase. We treat the pressure correction as an independent variable that is averaged as

$$\Delta\hat{p} = \frac{1}{2}(\Delta p_1 + \Delta p_2).$$

We assume constant compressibilities as described in Section 2.1. We may now easily check that the matrix

$$\hat{\mathbf{A}}(\mathbf{U}_1, \mathbf{U}_2) = \mathbf{A}(\hat{\mathbf{U}})$$

satisfies the weak Roe conditions R1–R3 when $\hat{\mathbf{U}}$ is in the hyperbolic region.

3.3.1. Numerical algorithm

Letting $\hat{\mathbf{A}}$ be diagonalized as

$$\hat{\mathbf{A}} = \mathbf{R}\boldsymbol{\Lambda}\mathbf{R}^{-1},$$

we write

$$\hat{\mathbf{A}}^{\pm} = \mathbf{R}\boldsymbol{\Lambda}^{\pm}\mathbf{R}^{-1},$$

where

$$\Lambda^{\pm} = \mathrm{diag}(\lambda_1^{\pm}, \lambda_2^{\pm}, \lambda_3^{\pm}, \lambda_4^{\pm}),$$

with

$$\lambda_i^{+} = \max(0, \lambda_i), \quad \lambda_i^{-} = \min(0, \lambda_i).$$

We now can write the scheme in the non-conservative form as

$$\mathbf{U}_j^{n+1} = \mathbf{U}_j^n - \frac{\Delta t}{\Delta x}\left(\mathbf{F}^{-}\left(\mathbf{U}_j^n, \mathbf{U}_{j+1}^n\right) + \mathbf{F}^{+}\left(\mathbf{U}_{j-1}^n, \mathbf{U}_j^n\right)\right) + \mathbf{Q}_j^n\Delta t, \tag{39}$$

where

$$\mathbf{F}^{\pm}(\mathbf{U}_j, \mathbf{U}_{j+1}) = \hat{\mathbf{A}}_{j+1/2}^{\pm}(\mathbf{U}_{j+1} - \mathbf{U}_j). \tag{40}$$

The numerical results produced by the Roe scheme, presented in Section 5, were obtained using a numerical algorithm to compute the eigenstructure of the Roe matrix.

4. Hybrid flux-splitting schemes

We will now describe an FVS and a van Leer scheme for the above two-fluid model, by adapting the schemes considered by Wada and Liou [35] for single-phase flow. In doing so, we will closely follow the approach that was previously used in [9] for a certain two-phase mixture model. Only the discretization of the non-conservative pressure term requires some special treatment, which will be discussed in more detail in Section 4.3.

We recall that for FVS the flux is split into upstream and downstream components as

$$\mathbf{F}(\mathbf{U}) = \mathbf{F}^{+}(\mathbf{U}) + \mathbf{F}^{-}(\mathbf{U}).$$

The numerical flux at the interface $j + 1/2$ is given as

$$\mathbf{F}_{j+1/2}(\mathbf{U}_{\mathrm{L}}, \mathbf{U}_{\mathrm{R}}) = \mathbf{F}^{+}(\mathbf{U}_{\mathrm{L}}) + \mathbf{F}^{-}(\mathbf{U}_{\mathrm{R}}). \tag{41}$$

The van Leer scheme is slightly different from the FVS scheme, since it introduces an upwind principle in the discretization of the momentum convective flux terms.

In the following, we will find it convenient to split the fluxes into convective and pressure parts and deal with each term separately. We write the system (4)–(7) as follows:

$$\frac{\partial \mathbf{U}}{\partial t} + \frac{\partial \mathbf{F}_{\mathrm{c}}}{\partial x} + \frac{\partial \mathbf{F}_{\mathrm{p}}}{\partial x} + \mathbf{H}\frac{\partial p_{\mathrm{i}}}{\partial x} = \mathbf{Q}, \tag{42}$$

where

$$\mathbf{Q} = \begin{bmatrix} 0 \\ 0 \\ Q_{\mathrm{g}} \\ Q_{\mathrm{l}} \end{bmatrix}, \quad \mathbf{H} = \begin{bmatrix} 0 \\ 0 \\ \alpha_{\mathrm{g}} \\ \alpha_{\mathrm{l}} \end{bmatrix}, \quad \mathbf{F}_{\mathrm{p}} = \begin{bmatrix} 0 \\ 0 \\ \alpha_{\mathrm{g}}\Delta p \\ \alpha_{\mathrm{l}}\Delta p \end{bmatrix} \quad \text{and} \quad \mathbf{F}_{\mathrm{c}} = \begin{bmatrix} \rho_{\mathrm{g}}\alpha_{\mathrm{g}}v_{\mathrm{g}} \\ \rho_{\mathrm{l}}\alpha_{\mathrm{l}}v_{\mathrm{l}} \\ \rho_{\mathrm{g}}\alpha_{\mathrm{g}}v_{\mathrm{g}}^2 \\ \rho_{\mathrm{l}}\alpha_{\mathrm{l}}v_{\mathrm{l}}^2 \end{bmatrix}.$$

We now consider discrete schemes in the form

$$\frac{\mathbf{U}_j^{n+1} - \mathbf{U}_j^n}{\Delta t} + \frac{[\mathbf{F}_{\mathrm{c}}]_{j+1/2}^n - [\mathbf{F}_{\mathrm{c}}]_{j-1/2}^n}{\Delta x} + \frac{[\mathbf{F}_{\mathrm{p}}]_{j+1/2}^n - [\mathbf{F}_{\mathrm{p}}]_{j-1/2}^n}{\Delta x} + \left[\mathbf{H}\frac{\partial p_{\mathrm{i}}}{\partial x}\right]_j^n = \mathbf{Q}_j^n. \tag{43}$$

4.1. Definition of numerical convective flux $[\mathbf{F}_c]_{j+1/2}$

A main feature of the splitting of the convective fluxes is the introduction of a local "convective" speed which will be defined such that the effects of sonic waves are included. That is, we define a splitting of the velocity v as

$$v = V^{+}(v, c) + V^{-}(v, c). \tag{44}$$

This splitting should satisfy a set of natural requirements as given by Liou [17]. We restate these requirements as

Assumption 1. Let the split velocity functions $V^{\pm}$ be chosen such that they satisfy the following requirements:
V1: *Consistency*. $V^+(v,c)+V^-(v,c)=v$.
V2: *Symmetry*. $V^+(v,c)=-V^-(v,c)$.
V3: *Left upwinding*. $V^+(v,c)=v$ for $v\geqslant c$.
Right upwinding. $V^-(v,c)=v$ for $v\leqslant -c$.
V4: *Differentiability*. $V^{\pm}$ are continuously differentiable.
V5: *Positivity*. $V^+(v,c)\geqslant 0$ and $V^-(v,c)\leqslant 0$.
V6: *Monotonicity*. $V^{\pm}$ are monotone increasing functions of v.

We note that for our model, the limits $v_k=\pm c$ do not generally correspond to sonic points where all eigenvalues become of the same sign. However, this correspondence is achieved in the limit $\varepsilon=0$ where the eigenvalues (30) become valid approximations. We therefore propose to introduce the approximate eigenvalues (30) as basis polynomials for the splitting formulas, as stated in Remark 1. We remark that practical applications of the two-fluid model deal mainly with the low Mach number domain and this approximation seems to work well in practice.

We then arrive at a direct generalization of the splitting formulas for the Euler equations

$$V^{\pm}(v,\hat{c})=\begin{cases}\pm\frac{1}{4\hat{c}}(v\pm\hat{c})^2 & \text{if } |v|\leqslant\hat{c},\\ \frac{1}{2}(v\pm|v|) & \text{otherwise.}\end{cases} \tag{45}$$

Following the standard set by earlier works [9,35], we chose a common sound velocity

$$\hat{c}_{j+1/2}=\max(\hat{c}_j,\hat{c}_{j+1}) \tag{46}$$

at the cell interface. The concept of a common velocity of sound will later allow us to modify the schemes to remove numerical dissipation at moving discontinuities associated with the volume fraction waves. This will be described in Section 4.4.

We are now in a position to define the numerical convective fluxes for our model.

(1) *Mass flux*. We let the numerical mass flux $(\rho\alpha v)_{j+1/2}$ be given as

$$(\rho\alpha v)_{j+1/2}=(\rho\alpha)_j V^+(v_j,\hat{c}_{j+1/2})+(\rho\alpha)_{j+1}V^-(v_{j+1},\hat{c}_{j+1/2}) \tag{47}$$

for each phase.

(2) *Momentum flux*. We let the numerical convective momentum flux $(\rho\alpha v^2)_{j+1/2}$ be given as

- FVS:

$$(\rho\alpha v^2)_{j+1/2}=V^+(v_j,\hat{c}_{j+1/2})(\rho\alpha v)_j+V^-(v_{j+1},\hat{c}_{j+1/2})(\rho\alpha v)_{j+1}, \tag{48}$$

- van Leer:

$$(\rho\alpha v^2)_{j+1/2}=\begin{cases}(\rho\alpha v)_{j+1/2}v_j & \text{if } (\rho\alpha v)_{j+1/2}\geqslant 0,\\ (\rho\alpha v)_{j+1/2}v_{j+1} & \text{otherwise}\end{cases} \tag{49}$$

or equivalently

$$(\rho\alpha v^2)_{j+1/2}=\frac{1}{2}(\rho\alpha v)_{j+1/2}(v_j+v_{j+1})-\frac{1}{2}\left|(\rho\alpha v)_{j+1/2}\right|(v_{j+1}-v_j). \tag{50}$$

We remark that the momentum flux constitutes the only difference between the FVS and van Leer schemes.

4.2. Definition of numerical pressure flux $[\mathbf{F}_p]_{j+1/2}$

Similar to the previous splitting of velocities, we introduce a weighting factor $P^{\pm}(v,c)$ designed to distribute the pressure waves into upstream and downstream travelling components. The weighting factor is normalized by

$$P^{+}(v,c)+P^{-}(v,c)=1.$$

Following Liou [17], we restate a set of natural requirements on such a weighting factor as follows.

Assumption 2. Let the split pressure functions $P^{\pm}$ be chosen such that they satisfy the following requirements:

P1: *Consistency*. $P^{+}(v,c)+P^{-}(v,c)=1$.
P2: *Symmetry*. $P^{+}(v,c)=P^{-}(-v,c)$.
P3: *Left upwinding*. $P^{+}(v,c)=1$ for $v>c$.
Right upwinding. $P^{-}(v,c)=1$ for $v<-c$.
P4: *Differentiability*. $P^{\pm}$ are continuously differentiable.
P5: *Positivity*. $P^{\pm}(v,c)\geqslant 0$.
P6: *Monotonicity*. $P^{\pm}$ are, respectively, monotone increasing and decreasing functions of v.

Again, using the approximate eigenvalue expression (30), we obtain the direct generalization of the splitting for the Euler equations

$$P^{\pm}(v,\hat{c})=V^{\pm}(v,\hat{c})\cdot\begin{cases}\frac{1}{\hat{c}}\left(\pm 2-\frac{v}{\hat{c}}\right) & \text{if } |v|\leqslant\hat{c},\\ \frac{1}{v} & \text{otherwise.}\end{cases}\tag{51}$$

Using this weighting factor, we split the conservative pressure flux $(\alpha\Delta p)_{j+1/2}$ as follows:

$$(\alpha\Delta p)_{j+1/2}=P^{+}(v_j,\hat{c}_{j+1/2})(\alpha\Delta p)_j+P^{-}(v_{j+1},\hat{c}_{j+1/2})(\alpha\Delta p)_{j+1}.\tag{52}$$

4.3. The non-conservative term

Now we focus on the non-conservative pressure term of (6) and (7) given by

$$\alpha_k\frac{\partial p^{\mathrm{i}}}{\partial x}=\alpha_k\frac{\partial}{\partial x}(p-\Delta p).\tag{53}$$

4.3.1. Consistency with non-conservative integrals

We propose discretizing the term (53) as

$$\left[\alpha_k\frac{\partial p^{\mathrm{i}}}{\partial x}\right]_j=\frac{1}{\Delta x}\left(F_{\mathrm{R}}(\mathbf{U}_j,\mathbf{U}_{j+1})-F_{\mathrm{L}}(\mathbf{U}_{j-1},\mathbf{U}_j)\right),\tag{54}$$

where we, as opposed to the conservative case, allow

$$F_{\mathrm{L}}(\mathbf{U}_j,\mathbf{U}_{j+1})\neq F_{\mathrm{R}}(\mathbf{U}_j,\mathbf{U}_{j+1}),$$

subject to the condition

$$F_{\mathrm{L}}(\mathbf{U},\mathbf{U})=F_{\mathrm{R}}(\mathbf{U},\mathbf{U})=0.\tag{55}$$

For a moment, let us assume that we have a stationary discontinuity in the pressure and volume fraction variable. We now aim to obtain expressions for F_L and F_R that will induce the "correct" momentum change over the assumed discontinuity in pressure and volume fraction. Correct in the sense that it is consistent with the description in Section 3.2 as expressed through the relations (34) and (37). For simplicity in notation we drop the indices k and i in the following.

Integrating (54) over a box containing only a discontinuity $(\mathbf{U}_1, \mathbf{U}_2)$ we obtain

$$F_R(\mathbf{U}_1, \mathbf{U}_2) - F_L(\mathbf{U}_1, \mathbf{U}_2) = \int_{\mathbf{U}_1}^{\mathbf{U}_2} \alpha \frac{\partial p}{\partial s} \, \mathrm{d}s = \bar{\alpha}(\alpha_1, \alpha_2)(p_2 - p_1), \tag{56}$$

relating the integral and discrete formulation of the model.

4.3.2. An FVS-like splitting

We propose to use an FVS-type splitting of the fluxes of the form

$$F_R(\mathbf{U}_1, \mathbf{U}_2) = F_R^+(\mathbf{U}_1, \bar{\alpha}) + F_R^-(\mathbf{U}_2, \bar{\alpha}) \tag{57}$$

and

$$F_L(\mathbf{U}_1, \mathbf{U}_2) = F_L^+(\mathbf{U}_1, \bar{\alpha}) + F_L^-(\mathbf{U}_2, \bar{\alpha}). \tag{58}$$

Inserting (57) and (58) into (56) we obtain the relation

$$F_R^+(\mathbf{U}_1, \bar{\alpha}) + F_R^-(\mathbf{U}_2, \bar{\alpha}) - F_L^+(\mathbf{U}_1, \bar{\alpha}) - F_L^-(\mathbf{U}_2, \bar{\alpha}) = \bar{\alpha}(\alpha_1, \alpha_2)(p_2 - p_1),$$

which suggests that $F_R^\pm$ and $F_L^\pm$ should satisfy the following relations:

$$F_L^+(\mathbf{U}, \bar{\alpha}) - F_R^+(\mathbf{U}, \bar{\alpha}) = \bar{\alpha} p,$$
$$F_L^-(\mathbf{U}, \bar{\alpha}) - F_R^-(\mathbf{U}, \bar{\alpha}) = -\bar{\alpha} p.$$

In addition, in view of (55), $F_R^\pm$ and $F_L^\pm$ should also satisfy

$$F_R^+(\mathbf{U}, \bar{\alpha}) = -F_R^-(\mathbf{U}, \bar{\alpha}),$$
$$F_L^+(\mathbf{U}, \bar{\alpha}) = -F_L^-(\mathbf{U}, \bar{\alpha}).$$

The following assumption summarizes these concerns and guarantees a treatment of a discontinuity in pressure and volume fraction consistent with the description in Section 3.2.

Assumption 3. Let the split non-conservative pressure fluxes $F_L^\pm$ and $F_R^\pm$ be chosen such that they satisfy the following requirements:
C1: $F_L^+(\mathbf{U}, \bar{\alpha}) + F_L^-(\mathbf{U}, \bar{\alpha}) = 0$.
C2: $F_R^+(\mathbf{U}, \bar{\alpha}) + F_R^-(\mathbf{U}, \bar{\alpha}) = 0$.
C3: $F_L^+(\mathbf{U}, \bar{\alpha}) + F_R^-(\mathbf{U}, \bar{\alpha}) = \bar{\alpha} p$.

Working within the framework of the pressure splitting functions which were applied in the discretization of the conservative pressure term as described in Section 4.2, some natural candidates for $F_L^\pm$ and $F_R^\pm$ are given by

$$F_L^\pm(\mathbf{U}, \bar{\alpha}) = \pm P^+(v, \hat{c}) \bar{\alpha} p^{\mathrm{i}} \tag{59}$$

and

$$F_R^\pm(\mathbf{U}, \bar{\alpha}) = \mp P^-(v, \hat{c}) \bar{\alpha} p^{\mathrm{i}}, \tag{60}$$

where $p^{\mathrm{i}} = p - \Delta p$ and where we use the same splitting formulas $P^{\pm}$ as given by (51). Note that the requirements C1 and C2 are trivially satisfied, whereas C3 is a consequence of the property P1 of Assumption 2 possessed by $P^{\pm}$. To sum up, we split the non-conservative pressure flux $(\alpha\partial_x p^{\mathrm{i}})_j$ as follows:

$$\begin{aligned}\left[\alpha\frac{\partial p^{\mathrm{i}}}{\partial x}\right]_j &= \frac{1}{\Delta x}\Big(F_{\mathrm{R}}(\mathbf{U}_j, \mathbf{U}_{j+1}, \bar{\alpha}_{j+1/2}) - F_{\mathrm{L}}(\mathbf{U}_{j-1}, \mathbf{U}_j, \bar{\alpha}_{j-1/2})\Big)\\ &= \frac{1}{\Delta x}\Big(\Big[\bar{\alpha}_{j-1/2}P^{+}(v_j, \hat{c}_{j-1/2})p_j^{\mathrm{i}} + \bar{\alpha}_{j+1/2}P^{-}(v_{j+1}, \hat{c}_{j+1/2})p_{j+1}^{\mathrm{i}}\Big]\\ &\qquad - \Big[\bar{\alpha}_{j-1/2}P^{+}(v_{j-1}, \hat{c}_{j-1/2})p_{j-1}^{\mathrm{i}} + \bar{\alpha}_{j+1/2}P^{-}(v_j, \hat{c}_{j+1/2})p_j^{\mathrm{i}}\Big]\Big),\end{aligned} \tag{61}$$

where we have used that F_{R} and F_{L} are given by (57)–(60), whereas $\bar{\alpha}_{j+1/2}$ is the average (37) discussed in Section 3.2

$$\bar{\alpha}_{j+1/2} = \frac{1}{2}(\alpha_j + \alpha_{j+1}). \tag{62}$$

Note that the last equality of (61) expresses that the discretization of $\alpha\partial_x p^{\mathrm{i}}$ on cell j is formed by using the weights $\bar{\alpha}_{j-1/2}$ and $\bar{\alpha}_{j+1/2}$ to defining appropriate averages of p at cell interface $j - 1/2$ as well as $j + 1/2$, and by that reflects the fact that α stands left of the differentiation operator. We also observe that the weighting of the discrete pressure values by means of the pressure splitting functions $P^{\pm}$ is similar to what we find in the discretization of the conservative pressure term as described by (52).

Remark 2. This straightforward analysis based on consistency with the definition of non-conservative integrals does not take velocities into account. The discontinuity is basically treated as stationary. However, an interesting property of the proposed splitting (61) is that it correctly yields a vanishing contribution for a case of uniform pressure ($p_j = p_{j+1}$) and velocity ($v_j = v_{j+1}$). As remarked in the end of the next section, this property ensures that the resulting schemes obey Abgrall's principle [1,28].

4.4. Removal of numerical dissipation

It is a well-known fact that the discretization of the FVS and van Leer scheme is excessively diffusive on the slow waves mainly responsible for mass transport, as too much emphasis is put on the sonic waves in the splitting formulas as given by (45). We refer to the previous analysis of the mixture model [9], where the same mass conservation equations are considered whereas a mixture momentum equation is used instead of two separate momentum equations. Consequently, we propose to use a similar mechanism for removing the excessive numerical dissipation as the one employed in [9].

In order to depict the main idea, we consider a contact discontinuity given by

$$\begin{aligned}&p_{\mathrm{L}} = p_{\mathrm{R}} = p,\\ &\alpha_{\mathrm{L}} \neq \alpha_{\mathrm{R}},\\ &(v_{\mathrm{g}})_{\mathrm{L}} = (v_{\mathrm{l}})_{\mathrm{L}} = (v_{\mathrm{g}})_{\mathrm{R}} = (v_{\mathrm{l}})_{\mathrm{R}} = v.\end{aligned} \tag{63}$$

Now $\varepsilon = 0$ as defined by (17) and the approximate eigenvalues (30) and (31) become exact. All pressure terms vanish from the model (4)–(7) and it is seen that the solution to this initial value problem is simply that the discontinuity will propagate with a velocity corresponding to the eigenvalue v. The exact solution of the Riemann problem will then give the numerical mass flux

$$(\rho\alpha v)_{j+1/2} = \frac{1}{2}\rho(\alpha_{\mathrm{L}} + \alpha_{\mathrm{R}})v - \frac{1}{2}\rho(\alpha_{\mathrm{R}} - \alpha_{\mathrm{L}})|v|. \tag{64}$$

Following Wada and Liou [35], we now let the splitting formulas $V^{\pm}$ be replaced by a more general pair $\tilde{V}^{\pm}$ which also involve the eigenvalue v in the polynomial expansion. That is, we write

$$\tilde{V}^{\pm}(v,c,\chi) = \begin{cases} \chi V^{\pm}(v,c) + (1-\chi)\frac{v\pm|v|}{2} & \text{if } |v| < c, \\ \frac{1}{2}(v \pm |v|) & \text{otherwise.} \end{cases} \tag{65}$$

We now restate the following lemma, which is proved in [9].

Lemma 1. *Let the velocity splittings* (65) *be used for the numerical mass fluxes* (47) *where a common velocity of sound* $\hat{c}_{j+1/2}$ *is assumed. Then, the exact Riemann solver flux* (64) *is recovered for the contact discontinuity given by* (63) *provided that the parameter* χ *of* (65) *satisfies*

$$\chi_R \alpha_R - \chi_L \alpha_L = 0. \tag{66}$$

In our previous work [9] on the mixture model, the simple choice

$$\chi_L = \alpha_R, \quad \chi_R = \alpha_L \tag{67}$$

was made. However, we observe that (66) allows for a degree of freedom in the choice of χ and the choice (67) may not be optimal. In particular, numerical investigations show that (67) does not work as well for the two-fluid model as it did for the more strongly coupled mixture model. A refinement of (67) will be presented in the following:

Scaling. First we wish to recover the FVS flux for the case $\mathbf{U}_L = \mathbf{U}_R$, to achieve maximum stability for continuous flow. That is, we want $\chi_L = \chi_R = 1$ for $\mathbf{U}_L = \mathbf{U}_R$. We may achieve this by the following rescaling

$$\chi_L = \frac{2\bar{\chi}_L}{\bar{\chi}_L + \bar{\chi}_R} \quad \text{and} \quad \chi_R = \frac{2\bar{\chi}_R}{\bar{\chi}_L + \bar{\chi}_R} = 2 - \chi_L, \tag{68}$$

where $\bar{\chi}_L$ and $\bar{\chi}_R$ are functions satisfying (66).

Pressure-dependent term. The analysis leading to Lemma 1 assumes uniform pressure. This means that we are free to introduce a pressure-dependent weighting factor into the expressions $\bar{\chi}_L$ and $\bar{\chi}_R$, writing them in the following form:

$$\bar{\chi}_L = \frac{w(p_L)}{\alpha_L}, \quad \bar{\chi}_R = \frac{w(p_R)}{\alpha_R}. \tag{69}$$

The purpose of the weighting factor $w(p)$ is to stabilize the scheme in the presence of pressure oscillations.

Finding a theoretical basis for the derivation of $w(p)$ is difficult. Wada and Liou [35] suggested the straightforward $w(p) = p$ for the Euler equations. This choice ensures a relative increase in the splitting velocity, and hence in the mass flux, from the cell containing the larger pressure. Other choices that could be considered are $w(p) = 1$ and $w(p) = p/\rho$. However, for the two-fluid model we consider here, we observed that better results are achieved by the weighting

$$w(p) = \rho(p). \tag{70}$$

This weighting factor ensures that only compressibility effects, as expressed by density differences across a pressure jump, are taken into account. It is justified by its performance in numerical experiments.

To summarize, we choose the following expressions for χ_L and χ_R:

$$\chi_L = \frac{2(\rho/\alpha)_L}{(\rho/\alpha)_L + (\rho/\alpha)_R}, \quad \chi_R = \frac{2(\rho/\alpha)_R}{(\rho/\alpha)_L + (\rho/\alpha)_R}. \tag{71}$$

Definition 1. Using the terminology of Wada and Liou [35], we will henceforth refer to the FVS scheme modified with the splittings (65) and the choice of χ described by (71) as the **AUSMV** scheme. That is, the AUSMV scheme is described by

- *Mass flux.*

$$(\rho\alpha v)_{j+1/2} = (\rho\alpha)_{\mathrm{L}}\tilde{V}^{+}(v_{\mathrm{L}}, \hat{c}_{j+1/2}, \chi_{\mathrm{L}}) + (\rho\alpha)_{\mathrm{R}}\tilde{V}^{-}(v_{\mathrm{R}}, \hat{c}_{j+1/2}, \chi_{\mathrm{R}}). \tag{72}$$

- *Momentum flux.*

$$(\rho\alpha v^2)_{j+1/2} = \tilde{V}^{+}(v_{\mathrm{L}}, \hat{c}_{j+1/2}, \chi_{\mathrm{L}})(\rho\alpha v)_{\mathrm{L}} + \tilde{V}^{-}(v_{\mathrm{R}}, \hat{c}_{j+1/2}, \chi_{\mathrm{R}})(\rho\alpha v)_{\mathrm{R}}. \tag{73}$$

The pressure terms are discretized as described in Sections 4.2 and 4.3.

Definition 2. Similarly, we will henceforth refer to the van Leer scheme modified with the splittings (65) and the choice of χ described by (71) as the **AUSMD** scheme. That is, the AUSMD scheme is described by

- *Mass flux.*

$$(\rho\alpha v)_{j+1/2} = (\rho\alpha)_{\mathrm{L}}\tilde{V}^{+}(v_{\mathrm{L}}, \hat{c}_{j+1/2}, \chi_{\mathrm{L}}) + (\rho\alpha)_{\mathrm{R}}\tilde{V}^{-}(v_{\mathrm{R}}, \hat{c}_{j+1/2}, \chi_{\mathrm{R}}). \tag{74}$$

- *Momentum flux.*

$$(\rho\alpha v^2)_{j+1/2} = \frac{1}{2}(\rho\alpha v)_{j+1/2}(v_{\mathrm{L}} + v_{\mathrm{R}}) - \frac{1}{2}|(\rho\alpha v)_{j+1/2}|(v_{\mathrm{R}} - v_{\mathrm{L}}). \tag{75}$$

The pressure terms are discretized as described in Sections 4.2 and 4.3.

As for the FVS and van Leer schemes, the only difference between AUSMV and AUSMD is their treatment of the convective momentum flux term. We note that neither the AUSMV nor the AUSMD scheme is a flux vector splitting (FVS) scheme as the numerical mass flux cannot be written in the form of (41).

Remark 3. According to the principle due to Abgrall [1,28], we want numerical schemes to obey the following physical principle: *A flow, uniform in pressure and velocity, must remain uniform in the same variables during its time evolution.*

In other words, if we had constant pressure and velocity everywhere in a flow at the time level t^n, then we will get the same pressure and velocity at the time t^{n+1}.

We now check if the AUSMV and AUSMD schemes obey Abgrall's priciple. Consequently, we assume that we have the contact discontinuity given by (63) and that it remains unchanged during the time interval $[t^n, t^{n+1}]$. In view of Definitions 1 and 2, we immediately can conclude that the mass equations and the momentum equations take the form

$$(\rho\alpha)_j^{n+1} = (\rho\alpha)_j^n - \frac{\Delta t}{\Delta x}\left((\rho\alpha v)_{j+1/2}^n - (\rho\alpha v)_{j-1/2}^n\right),$$

$$v(\rho\alpha)_j^{n+1} = v(\rho\alpha)_j^n - v\frac{\Delta t}{\Delta x}\left((\rho\alpha v)_{j+1/2}^n - (\rho\alpha v)_{j-1/2}^n\right) - \frac{\Delta t}{\Delta x}\left((\alpha\Delta p)_{j+1/2}^n - (\alpha\Delta p)_{j-1/2}^n\right) - \Delta t\left[\alpha\frac{\partial p^{\mathrm{i}}}{\partial x}\right],$$

where $(\rho\alpha v)_{j+1/2}^n$ is in the form (64). From (52) and (11) we see that $(\alpha\Delta p)_{j+1/2}^n = 0$, whereas it follows from (61) that $[\alpha\frac{\partial p^{\mathrm{i}}}{\partial x}] = 0$. Consequently, the pressure terms vanish and we conclude that the AUSMV and AUSMD schemes satisfy Abgrall's principle.

5. Numerical simulations

In the following, some selected numerical examples will be presented. As our main concern will be to demonstrate the inherent accuracy and stability properties of the different schemes, we limit ourselves to first order accuracy in space and time. Explicit time integration is used.

5.1. Shock tube problems

Shock tube problems are interesting for the following reasons:

- They test the ability of numerical schemes to handle initial data that are far removed from an equilibrium state.
- The existence of discontinuities in both volume fraction and pressure provides a test that numerical schemes converge to the same weak solutions in the presence of the non-conservative terms.

In this section, we will investigate a couple of shock tube problems where the relative velocity between the phases is rather large. This provides a test of the validity of using approximate eigenvalues as basis polynomials for the splitting formulas, as described in Remark 1.

5.1.1. Shock tube problem 1

We consider an initial Riemann problem also investigated by Cortes et al. [6] for a similar two-fluid model. The initial states are given by

$$\mathbf{W}_{\mathrm{L}} = \begin{bmatrix} p \\ \alpha_{\mathrm{l}} \\ v_{\mathrm{g}} \\ v_{\mathrm{l}} \end{bmatrix} = \begin{bmatrix} 265,000\ \mathrm{Pa} \\ 0.71 \\ 65\ \mathrm{m/s} \\ 1\ \mathrm{m/s} \end{bmatrix} \tag{76}$$

and

$$\mathbf{W}_{\mathrm{R}} = \begin{bmatrix} p \\ \alpha_{\mathrm{l}} \\ v_{\mathrm{g}} \\ v_{\mathrm{l}} \end{bmatrix} = \begin{bmatrix} 265,000\ \mathrm{Pa} \\ 0.7 \\ 50\ \mathrm{m/s} \\ 1\ \mathrm{m/s} \end{bmatrix}. \tag{77}$$

We used the timestep $\Delta x/\Delta t = 10^3$ m/s and a computational grid of 100 cells. The results, plotted at the time $T = 0.1$ s, are given in Figs. 1 and 2. The reference solution was computed using the Roe scheme on a fine grid of 10,000 cells. The existence of two separate volume fraction waves can be seen from the small wedge in liquid fraction at $x = 50$ m, which appears clearly only in the reference solution.

We make the following observations:

- The FVS and van Leer schemes are able to produce stable and non-oscillatory approximations. As expected, they are excessively diffusive on the slow volume fraction waves. The van Leer scheme is more accurate than FVS on liquid velocity.
- The AUSMV and AUSMD produce a resolution of sonic waves which is comparable to that of FVS and van Leer. However, the slow volume fraction waves are reproduced with less numerical diffusion. The price to pay is that some oscillations around the volume fraction discontinuities are introduced by AUSMV. More severe oscillations, which are particularly visible for the liquid velocity, occur for AUSMD.

For this problem, it was noted that the oscillations produced by AUSMD developed into instabilities as the grid was refined. However, the oscillations observed for AUSMV would decay with grid refinement. This is demonstrated in Fig. 3, where AUSMV on a grid of 50,000 cells is compared to the Roe reference solution. The two solutions are virtually identical.

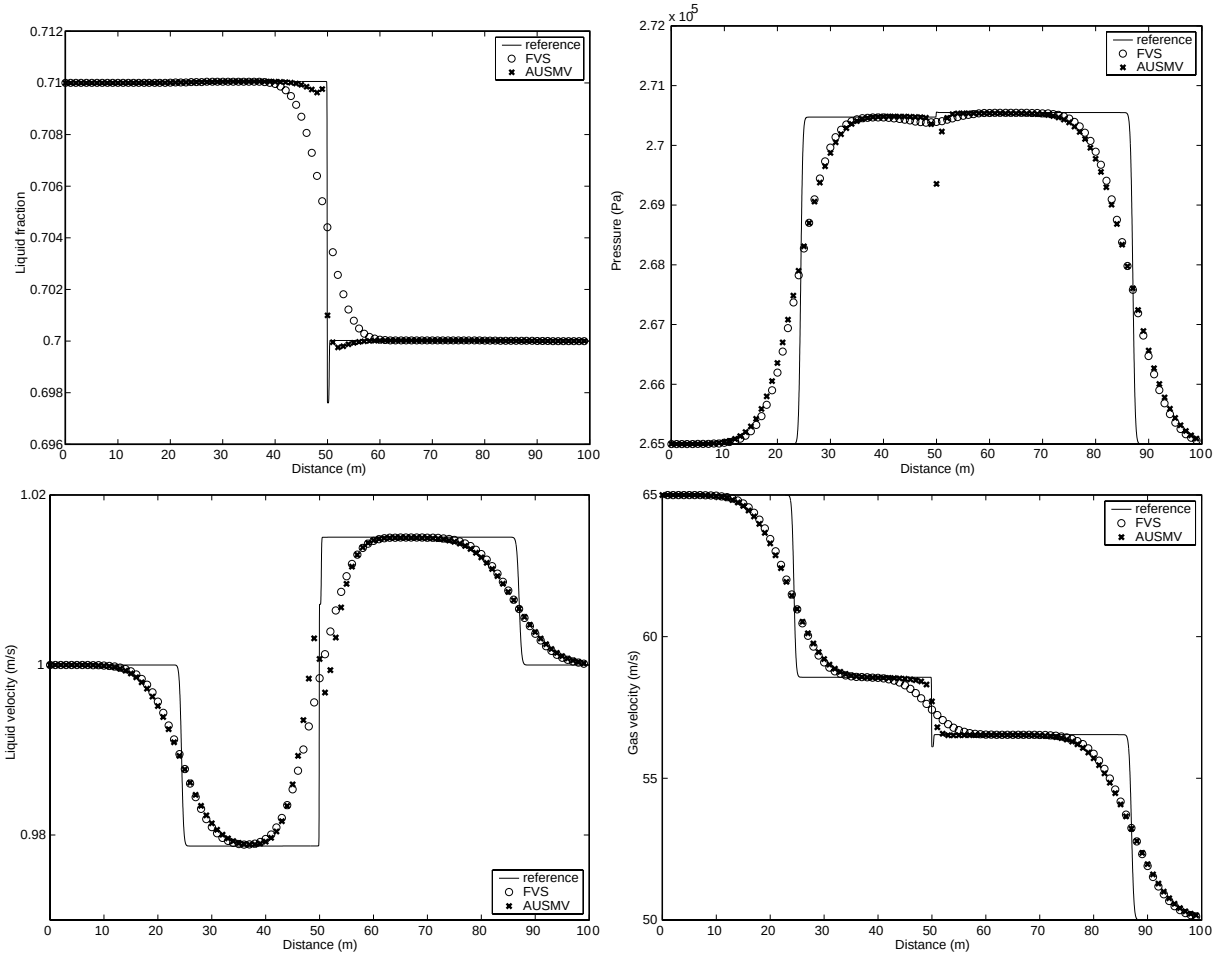

Fig. 1. Shock tube problem 1. FVS and AUSMV scheme on a grid of 100 cells. Top left: liquid fraction. Top right: pressure. Bottom left: liquid velocity. Bottom right: gas velocity.

5.1.2. Shock tube problem 2

We now consider a problem similar to shock tube problem 1, but with a bigger volume fraction jump and a jump also in the liquid velocity. The initial states are given by

$$\mathbf{W}_{\mathrm{L}} = \begin{bmatrix} p \\ \alpha_{\mathrm{l}} \\ v_{\mathrm{g}} \\ v_{\mathrm{l}} \end{bmatrix} = \begin{bmatrix} 265{,}000\ \mathrm{Pa} \\ 0.7 \\ 65\ \mathrm{m/s} \\ 10\ \mathrm{m/s} \end{bmatrix} \tag{78}$$

and

$$\mathbf{W}_{\mathrm{R}} = \begin{bmatrix} p \\ \alpha_{\mathrm{l}} \\ v_{\mathrm{g}} \\ v_{\mathrm{l}} \end{bmatrix} = \begin{bmatrix} 265{,}000\ \mathrm{Pa} \\ 0.1 \\ 50\ \mathrm{m/s} \\ 15\ \mathrm{m/s} \end{bmatrix}. \tag{79}$$

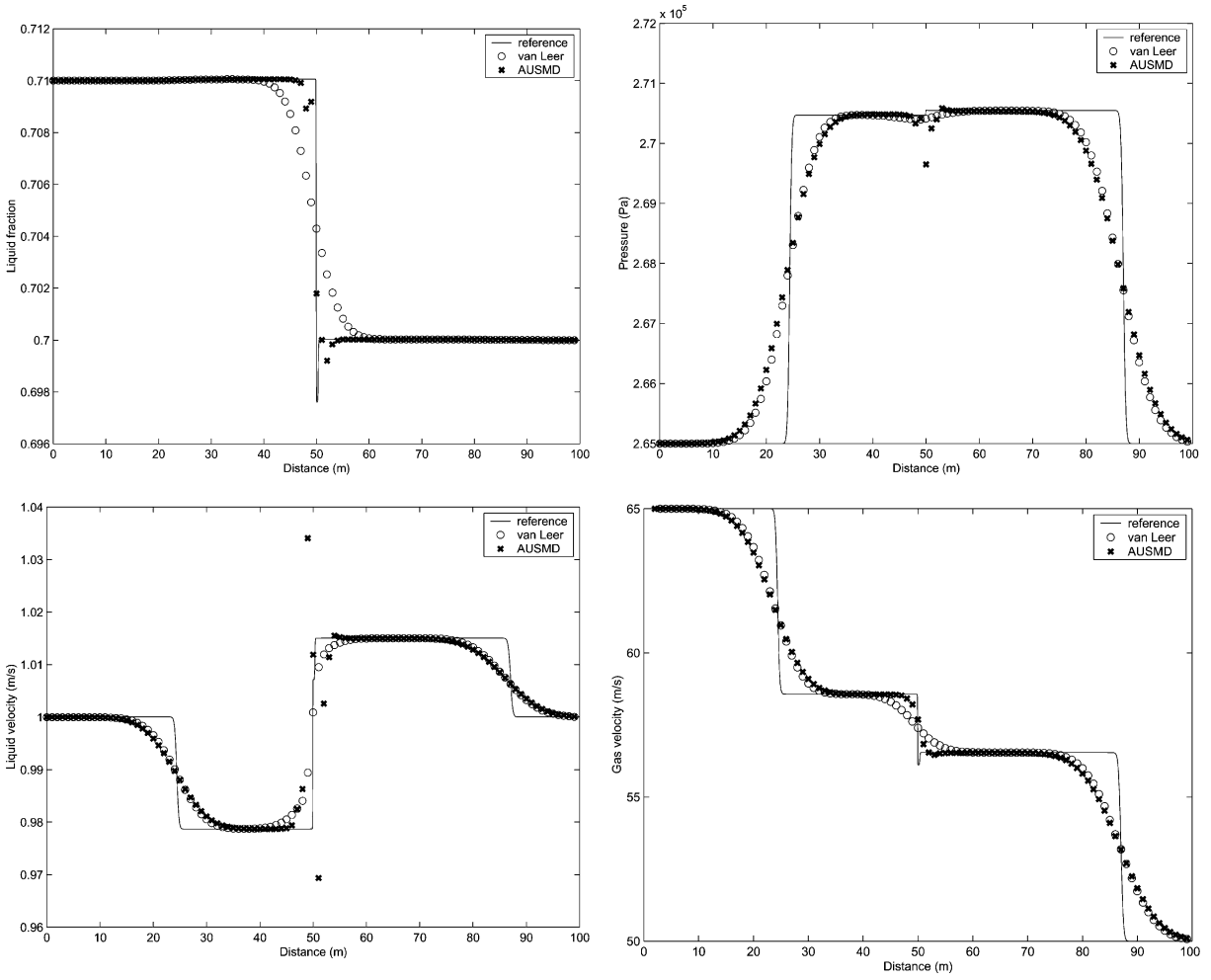

Fig. 2. Shock tube problem 1. Comparison between van Leer and AUSMD scheme on a grid of 100 cells. Top left: liquid fraction. Top right: pressure. Bottom left: liquid velocity. Bottom right: gas velocity.

Using a timestep of $\Delta x/\Delta t = 750$ m/s, results for AUSMV are plotted in Fig. 4 for gradually finer grids. Similar results for AUSMD are plotted in Fig. 5. As for shock tube problem 1, the reference solution was computed by the Roe scheme using a grid of 10,000 cells.

The volume fraction variable is largely unaffected by the pressure waves. We have therefore magnified the volume fraction plots, focusing on the slow-moving volume fraction waves instead. The number of grid cells in the legend refers to the number of cells visible in the plots.

This problem does not display an essential difference in the stability properties of AUSMV and AUSMD. However, we note that the AUSMD scheme produces more accurate solutions for liquid velocity than AUSMV.

It is interesting that both AUSMV and AUSMD seem to produce the same wave structure in the volume fraction variable as the Roe scheme. This structure arises due to the existence of two separate volume fraction waves, as described in Section 3.1. This is a nonlinear effect that is not taken into consideration by the splitting formulas, which are based on the approximate eigenvalues stated in Remark 1.

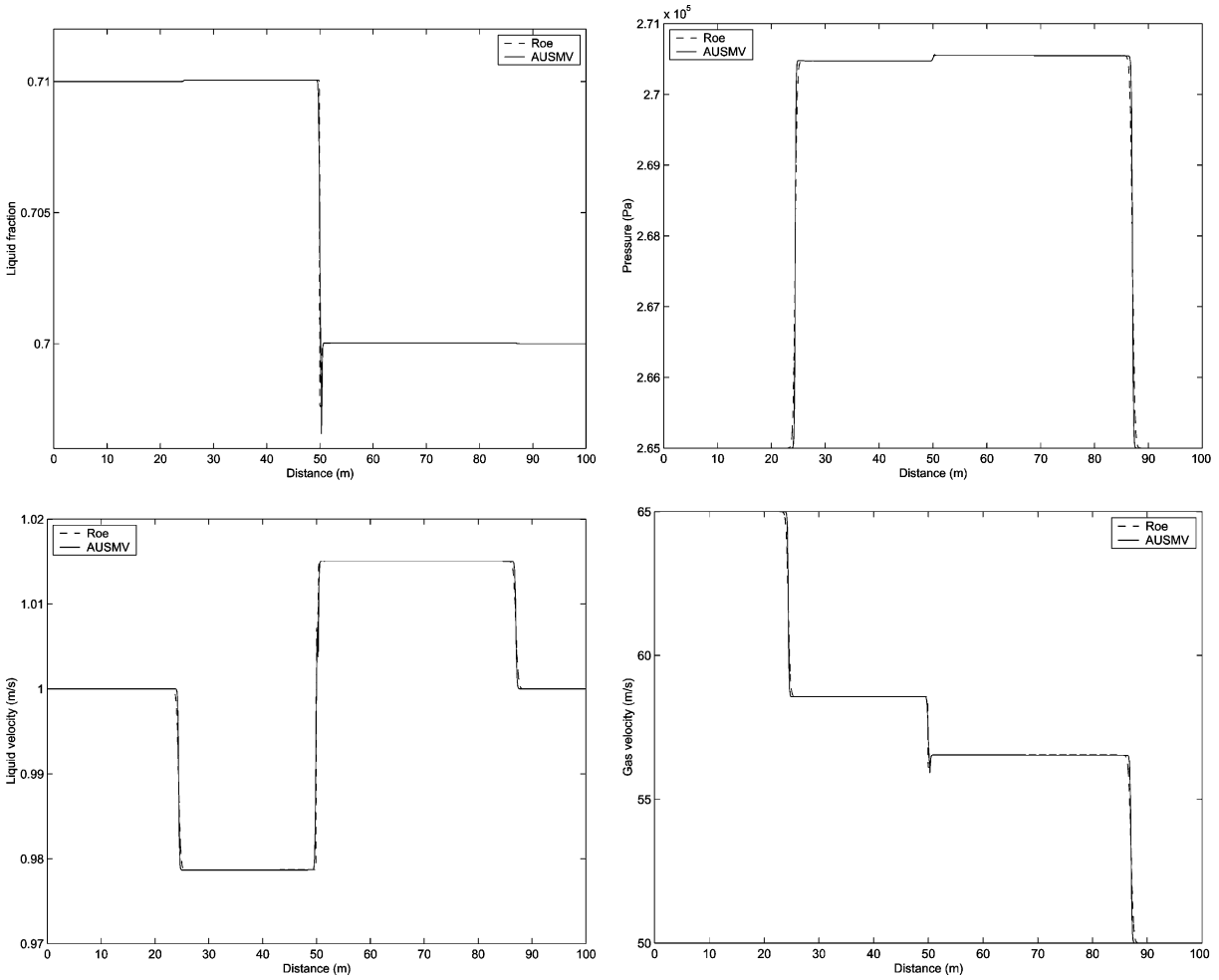

Fig. 3. Shock tube problem 1. Convergence of Roe and AUSMV schemes. Top left: liquid fraction. Top right: pressure. Bottom left: liquid velocity. Bottom right: gas velocity.

5.1.3. Preliminary conclusions

To summarize the results of this section, we have observed:

- The FVS and van Leer schemes provide non-oscillatory numerical solutions around discontinuities.
- AUSMV and AUSMD are less diffusive on volume fraction waves than the FVS and van Leer schemes. Stability problems may occur for AUSMD. AUSMV is stable.
- The AUSMV and Roe scheme seem to converge to the same solutions. This is also in accordance with observations made in [9] for a two-phase mixture model. Particularly, these numerical tests provide a justification of the discretization of the non-conservative pressure term as described in Section 4.3.

Remark 4. The oscillations observed for AUSMV and AUSMD indicate that these schemes do not have the "Total Variation Diminishing" property. As described in Section 3.1, the wave structure of the model involves strong couplings between the phasic variables. Such couplings are naturally incorporated in approximate Riemann solvers like the Roe scheme, which take the full eigenstructure into account to

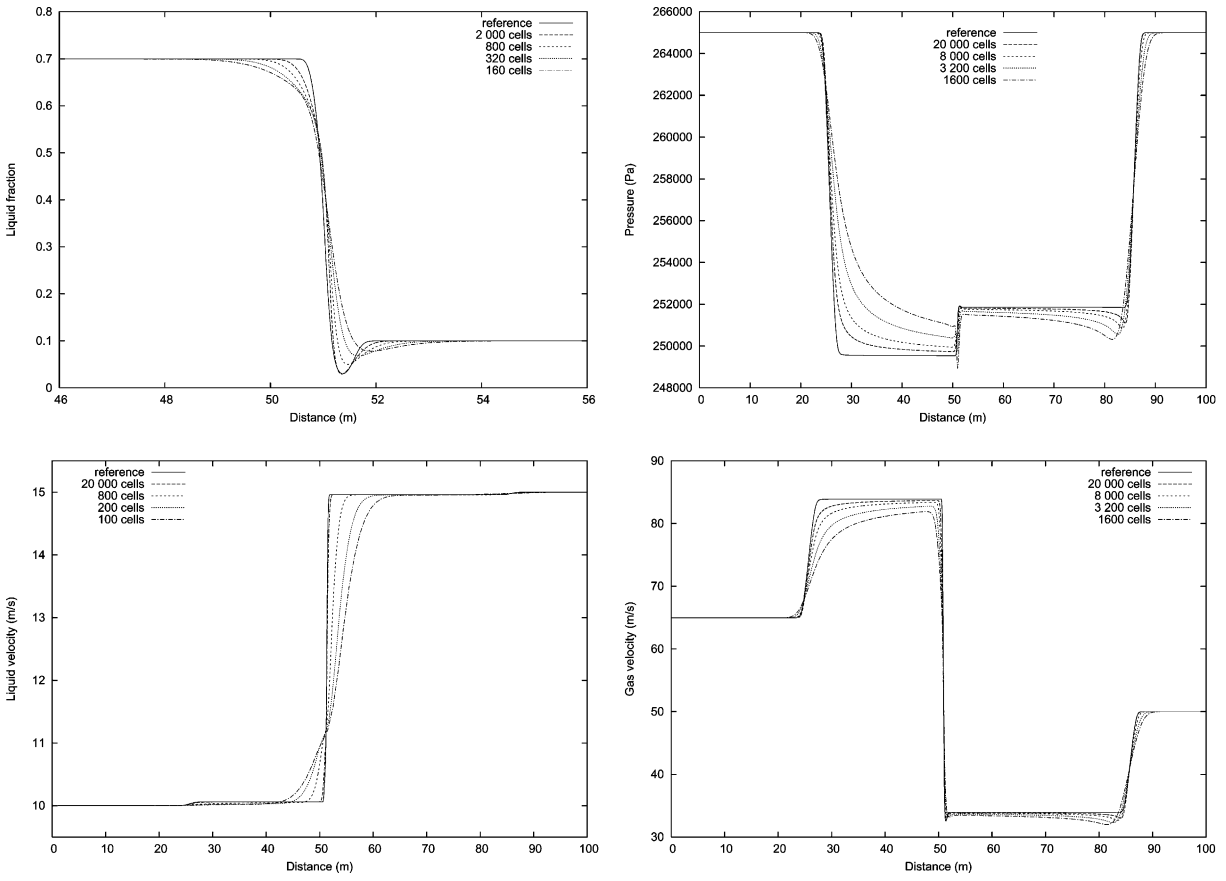

Fig. 4. Shock tube problem 2. Grid refinement for the AUSMV scheme. Top left: liquid fraction. Top right: pressure. Bottom left: liquid velocity. Bottom right: gas velocity.

determine the flux splittings. However, the splitting formulas given by (65) and (71) involve phasic couplings only in the common sound velocity. This simplification may partly explain the loss of monotonicity observed for AUSMV and AUSMD.

5.2. Water faucet

We now consider a simplified faucet flow problem proposed by Ransom [24]. This problem has previously been used by several authors for testing the ability of numerical schemes to accurately resolve volume fraction fronts [5,21,23,33,34] and has become a standard benchmark. We consider a vertical pipe of length 12 m with the initial uniform state

$$\mathbf{W} = \begin{bmatrix} p \\ \alpha_{\mathrm{l}} \\ v_{\mathrm{g}} \\ v_{\mathrm{l}} \end{bmatrix} = \begin{bmatrix} 10^5 \text{ Pa} \\ 0.8 \\ 0 \\ 10 \text{ m/s} \end{bmatrix}. \tag{80}$$

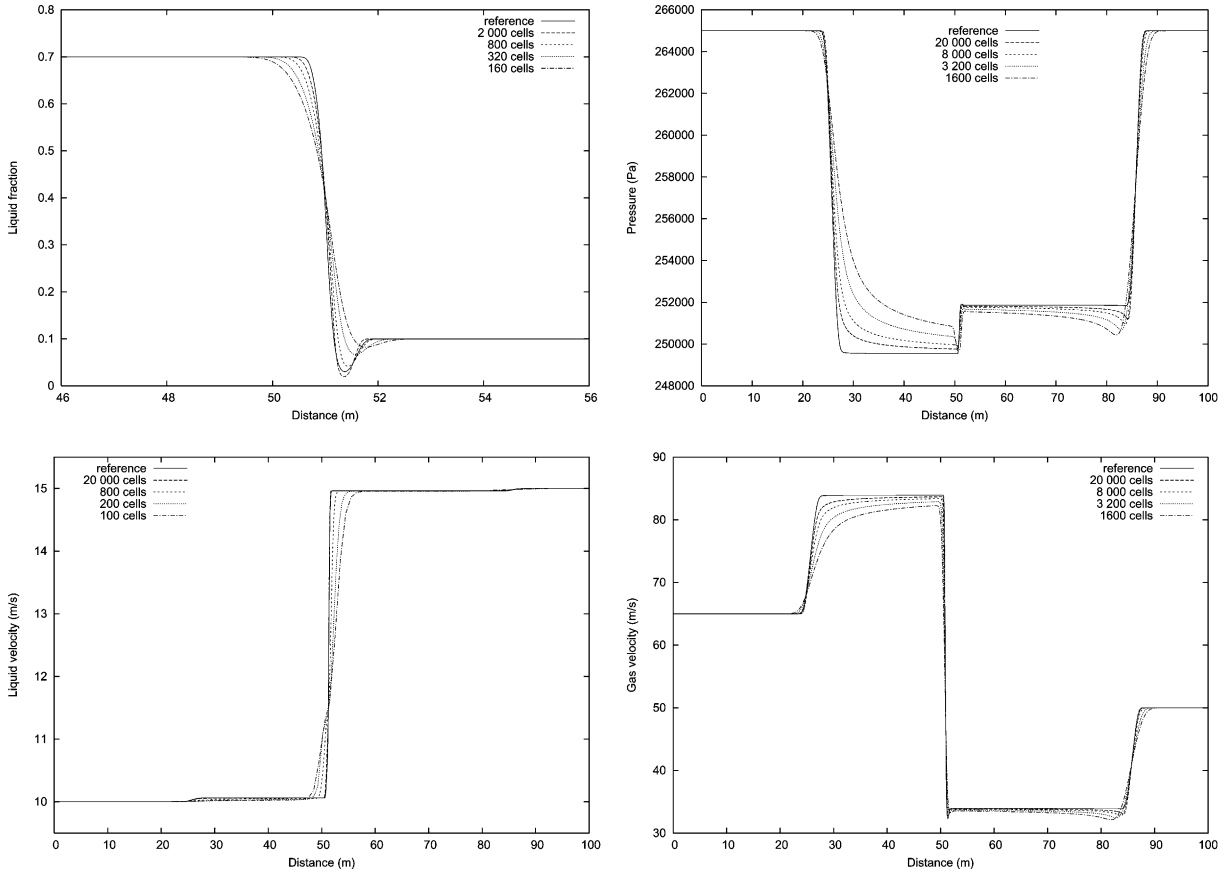

Fig. 5. Shock tube problem 2. Grid refinement for the AUSMD scheme. Top left: liquid fraction. Top right: pressure. Bottom left: liquid velocity. Bottom right: gas velocity.

Gravity is the only source term taken into account, i.e., in the framework of (6) and (7) we have

$$Q_k = g\rho_k\alpha_k, \tag{81}$$

with g being the acceleration of gravity. At the inlet, we have the constant conditions $\alpha_l = 0.8$, $v_l = 10$ m/s and $v_g = 0$. At the outlet, the pipe is open to the ambient pressure $p = 10^5$ Pa. We determined the remaining variables at the boundaries by simple extrapolation.

Ransom noted that an analytical solution for volume fraction and liquid velocity can be found assuming that the pressure variation in the vapor phase can be ignored. The procedure is described by Trapp and Riemke [34], here we provide only the result

$$v_l(x,t) = \begin{cases} \sqrt{v_0^2 + 2gx} & \text{for } x < v_0 t + \frac{1}{2}gt^2, \\ v_0 + gt & \text{otherwise.} \end{cases} \tag{82}$$

$$\alpha_l(x,t) = \begin{cases} \alpha_0\left(1 + 2gxv_0^{-2}\right)^{-1/2} & \text{for } x < v_0 t + \frac{1}{2}gt^2, \\ \alpha_0 & \text{otherwise.} \end{cases} \tag{83}$$

The parameters $\alpha_0 = 0.8$ and $v_0 = 10$ m/s are the initial states.

Remark 5. This solution is not "analytical" in the sense that the model (4)–(6) is solved exactly by analysis. Rather, it is "analytical" in the sense that the approximate solutions (82) and (83) are given in terms of analytical expressions. However, the simplifying assumption leading to these analytical expressions is valid to a high degree of accuracy and we expect these approximate solutions to be virtually inseparable from the real solutions to the full model.

5.2.1. Test of accuracy of the different schemes on volume fraction

In Fig. 6, the gas volume fraction is plotted for $T = 0.6$ s for a grid of 120 computational cells. The different schemes are plotted together for the sake of comparison. We observe that

- The van Leer scheme is more accurate than FVS. This is consistent with our findings for shock tube problem 1.
- AUSMV and AUSMD are both more accurate than the van Leer scheme. AUSMD is more accurate than AUSMV. The accuracy of AUSMD is comparable to that of the Roe scheme.

5.2.2. Results for hybrid flux-splitting schemes

For the AUSMD/V and Roe schemes, the full set of variables are plotted in Fig. 7. For the reference solution the approximate analytical solution was used to calculate volume fraction and liquid velocity, while the Roe scheme on a finer grid (1200 cells) was used to calculate the pressure and gas velocity. A notable fact is that severe oscillations, as were observed for AUSMD on shock tube problem 1, do not occur. In fact, AUSMD gives a resolution comparable to the Roe scheme also on the velocities.

5.2.3. Convergence comparison

A more detailed look at the accuracy of the schemes regarding the volume fraction is given in Fig. 8. This figure demonstrates the fundamental difference in the dissipative mechanism of AUSMD and AUSMV. In particular, we note that AUSMD is approximately as accurate as AUSMV calculated on a grid size whose

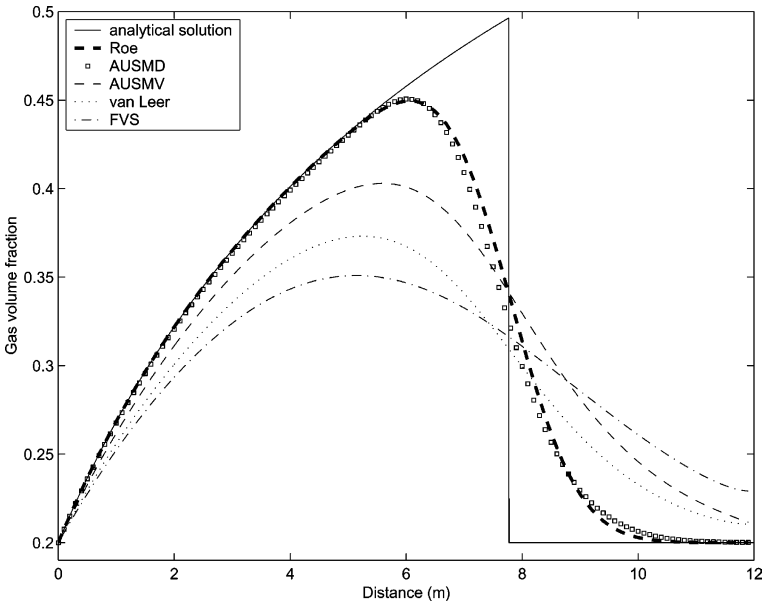

Fig. 6. Water faucet. $T = 0.6$ s. Resolution of volume fraction for Roe, AUSMD, AUSMV, van Leer, and FVS schemes on a grid of 120 cells.

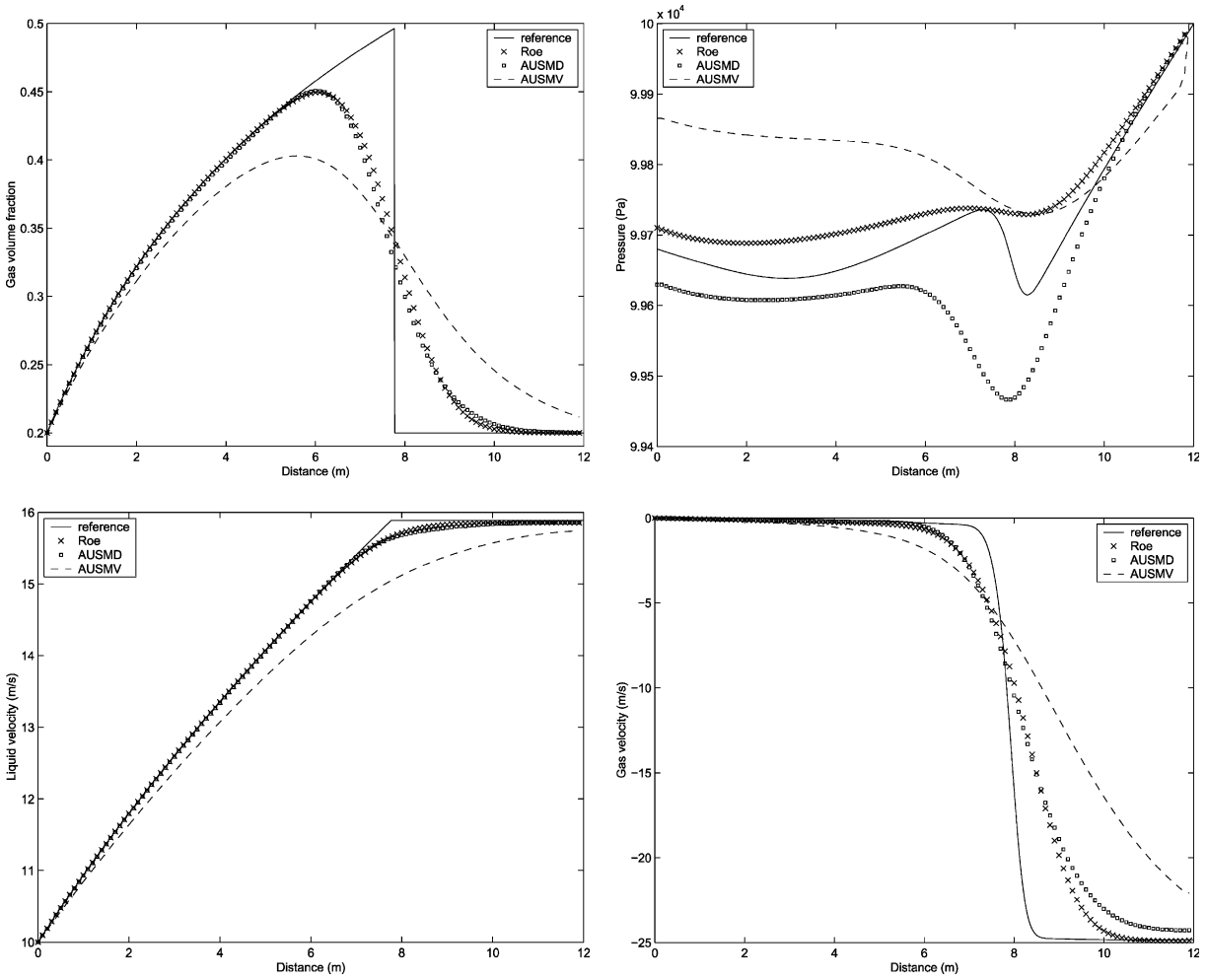

Fig. 7. Water faucet. $T = 0.6$ s. Roe, AUSMD and AUSMV schemes on a grid of 120 cells. Top left: liquid fraction. Top right: pressure. Bottom left: liquid velocity. Bottom right: gas velocity.

magnitude differs by one order. We also note that for the case with 1200 cells, AUSMD has introduced a slight overshoot in the approximation of the volume fraction. This is a manifestation of the weaker dissipative mechanism of AUSMD.

Remark 6. One may wonder whether simpler choices for the splitting formulas would work, for instance, for the water faucet problem. In [10], it was observed that simpler choices produced good results for typical mass transport problems described by a two-phase model consisting of two mass conservation equations and a mixture momentum equation. However, for the current two-fluid model where the coupling between the phasic velocities is much looser, it seems that the introduction of the sound velocity in the splitting formulas (45) and (51) is very essential. Neglecting the sound velocity and using pure advective upwinding

$$V^{\pm}(v,c) = \frac{1}{2}(v \pm |v|),$$

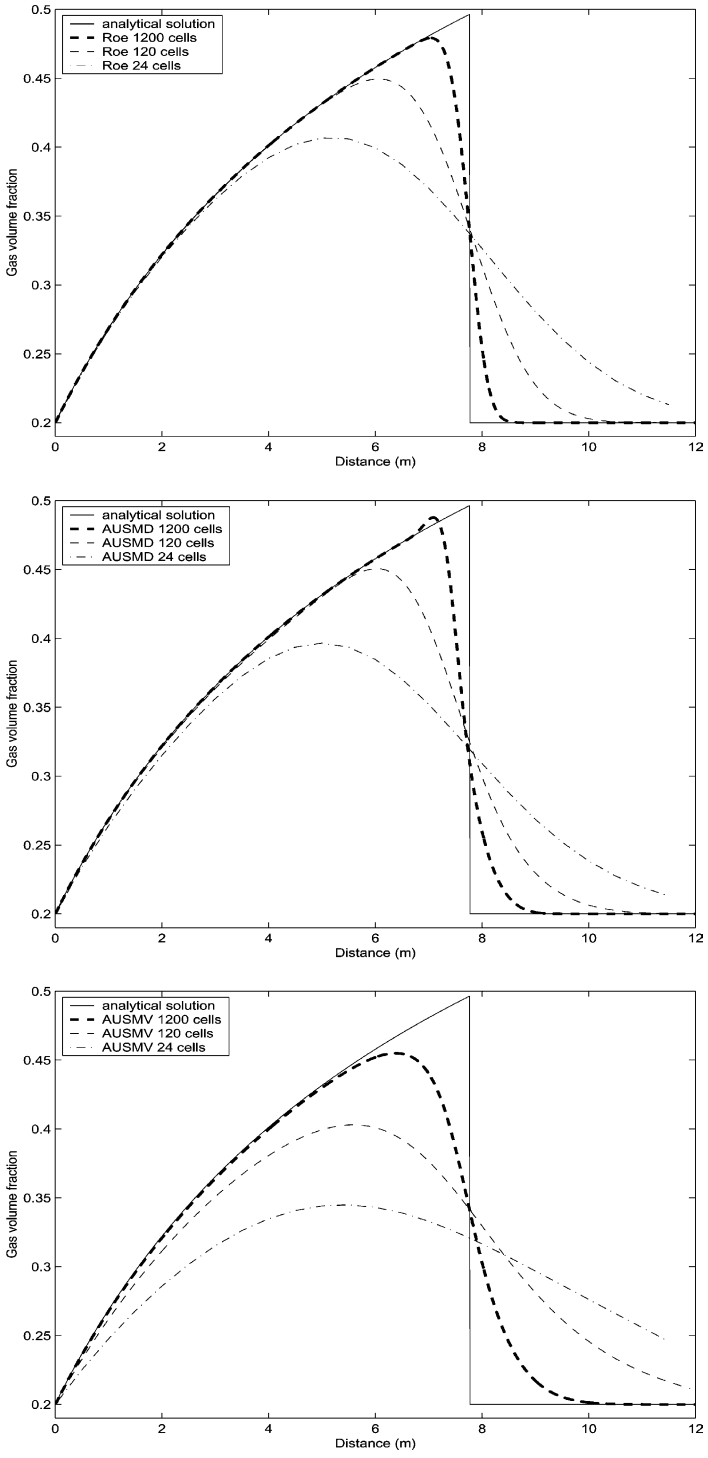

Fig. 8. Water faucet. $T = 0.6$ s. Accuracy on volume fraction. Top: grid refinement for Roe scheme. Center: grid refinement for AUSMD scheme. Bottom: grid refinement for AUSMV scheme.

as well as central pressure splitting

$$P^{\pm}(v,c)=\frac{1}{2}$$

were found to cause severe instabilities.

5.3. Transition to one-phase flow

It is seen that the model (4)–(7) becomes singular in the limits $\alpha_k \to 0$ ($k = \mathrm{g},\mathrm{l}$), corresponding to the transition to one-phase flow. Stability problems are commonly encountered as this limit is approached. We observed that our implementation of the Roe scheme could not handle this in a satisfactory manner, and Coquel et al. [5] report instabilities for their Riemann-free upwind scheme based on kinetic considerations, occurring for values of α_k near 10^{-6}. They suggested a modification of the discretization of the non-conservative term to solve this problem.

Indeed, a similar problem was also observed for the AUSMD and AUSMV schemes and a fix is required. We suggest a method consistent with the framework we are working within, leaving the non-conservative term unaffected. Our suggestion is based on the following observations:

- The resolution of sonic waves is very similar for the FVS/van Leer and the AUSMV/D schemes. The van Leer and FVS schemes seem to be able to deal with the transition to one-phase flow in a stable manner, whereas AUSMV/D typically become unstable.
- The volume fraction waves disappear in the one-phase limit of the system. Hence, the effect of volume fraction waves is expected to disappear as a phase fraction tends to zero and the dynamics will be dominated by pressure waves.

This naturally suggests removing the advective velocity contribution to (65), falling back to the splitting (45) in near one-phase regions. We achieve this by replacing (71) by the following expressions:

$$\chi_{\mathrm{L}}=(1-\phi_{\mathrm{L}})\frac{2(\rho/\alpha)_{\mathrm{L}}}{(\rho/\alpha)_{\mathrm{L}}+(\rho/\alpha)_{\mathrm{R}}}+\phi_{\mathrm{L}} \tag{84}$$

and

$$\chi_{\mathrm{R}}=(1-\phi_{\mathrm{R}})\frac{2(\rho/\alpha)_{\mathrm{R}}}{(\rho/\alpha)_{\mathrm{L}}+(\rho/\alpha)_{\mathrm{R}}}+\phi_{\mathrm{R}} \tag{85}$$

for both phases. Here, ϕ is a smooth symmetric function $\phi(\alpha)=\phi(1-\alpha)$ designed to be 1 near one-phase regions and 0 otherwise. A simple expression having this property is

$$\phi=\phi(\alpha_{\mathrm{g}})=\frac{1}{\mathrm{e}^{k\alpha_{\mathrm{g}}}}+\frac{1}{\mathrm{e}^{k(1-\alpha_{\mathrm{g}})}}, \tag{86}$$

where the parameter k determines the degree of smoothness of ϕ. We found the value

$$k=200 \tag{87}$$

to be a good compromise, providing both a smooth and accurate transition mechanism.

Definition 3. The modification of the AUSMV scheme obtained by replacing (71) in Definition 1 by (84) and (85) will be denoted as the $AUSMV^{*}$ scheme. Similarly, the modification of the AUSMD scheme obtained by replacing (71)in Definition 2 by (84) and (85) will be denoted as the $AUSMD^{*}$ scheme.

Remark 7. The property of AUSMD and AUSMV of reproducing the exact Riemann solver mass flux is formally lost by this modification. However, the flux modification is significant only for near one-phase regions where we expect little loss of accuracy. In particular, for the shock tube and water faucet examples considered so far, $\phi < 10^{-17}$ and the results are unchanged to plotting accuracy.

5.3.1. AUSMDV

We observed that the van Leer and AUSMD* schemes could handle a smooth transition to one-phase flow. We also observed that if the transition is very abrupt, the van Leer and AUSMD* schemes could fail. However, the FVS and AUSMV* schemes seem stable also for such situations.

This demonstrates the need for a more sophisticated hybridization where we want to combine the accuracy of AUSMD* with the stability of AUSMV*. Based on our observations so far, we note the following:

- The FVS scheme possesses outstanding stability properties. The AUSMV scheme largely keeps these properties, and with the transition fix (84) and (85), AUSMV* seems to be able to handle very general flow conditions without introducing instabilities.
- The AUSMD has a weak dissipation mechanism allowing it to resolve discontinuities with an accuracy comparable to the Roe scheme. However, it is more prone to produce instabilities and overshoots.

This naturally suggests combining the AUSMD and AUSMV fluxes as follows:

$$F_c^{\mathrm{AUSMDV}} = sF_c^{\mathrm{AUSMV}} + (1-s)F_c^{\mathrm{AUSMD}}, \tag{88}$$

where s is some parameter. We remark that only the convective flux in the momentum equations will be affected by this modification.

For the parameter s many choices are possible. As the previous examples show, the optimal choice might be problem-dependent. For one-phase flow, Wada and Liou [35] suggested letting s depend on the local pressure gradient, and similar ideas may be fruitful here.

We will not discuss this issue in full depth, but proceed to demonstrate that a simple choice for s will make the AUSMDV able to handle a stiff transition to one-phase flow in a stable and accurate manner. We observe that for a typical interface problem the strong gradients are associated only with the transition points between one-phase and two-phase flow. We consequently propose to use

$$s = \max(\phi_L, \phi_R), \tag{89}$$

where ϕ is given by (86). In particular, we note that this choice of s will make AUSMDV reduce to AUSMD for the water faucet and shock tube problems.

Definition 4. The scheme obtained by combining the AUSMV* and AUSMD* convective momentum fluxes is as follows:

$$F_c^{\mathrm{AUSMDV}^*} = sF_c^{\mathrm{AUSMV}^*} + (1-s)F_c^{\mathrm{AUSMD}^*}, \tag{90}$$

where s is given by (89), will be denoted as the **AUSMDV*** scheme.

We note that AUSMDV* basically reduces to the stable FVS scheme near one-phase regions and the accurate AUSMD scheme elsewhere.

It seems that this approach can provide a good basis for methods aiming to resolve practical problems related to mass transport of oil and gas in pipelines. For such problems, the main dynamics are associated with slow transients and strong discontinuities are expected to occur only at the transition points to one-phase flow. Such discontinuities will commonly be induced by the buildup of liquid slugs due to gravity.

5.4. Separation problem

To illustrate the effect of the transition fix described above, we consider a simplified gravity-induced phase separation problem proposed by Coquel et al. [5]. For this problem the transition from two-phase to one-phase flow occurs under stiff conditions, providing a good test for the stability of the schemes.

We consider a vertical pipe of length 7.5 m, where, as for the water faucet problem, gravity is the only source term taken into account. Initially, the pipe is filled with stagnant liquid and gas with a uniform pressure of $p = 10^5$ Pa and a uniform liquid fraction of $\alpha_l = 0.5$. The pipe is considered to be closed at both ends, i.e., both phasic velocities are forced to be zero at the end points. Assuming that the pressure variation can be neglected, an analytical solution can be derived in a similar manner as for the water faucet. We assume that the liquid is accelerated by gravity only until it is abruptly brought into stagnant conditions at the lower part of the tube. This yields the following approximate analytical solution for liquid velocity and volume fraction:

$$v_l(x,t) = \begin{cases} \sqrt{2gx} & \text{for } x < \frac{1}{2}gt^2, \\ gt & \text{for } \frac{1}{2}gt^2 \leqslant x < L - \frac{1}{2}gt^2, \\ 0 & \text{for } L - \frac{1}{2}gt^2 < x, \end{cases} \tag{91}$$

$$\alpha_l(x,t) = \begin{cases} 0 & \text{for } x < \frac{1}{2}gt^2, \\ 0.5 & \text{for } \frac{1}{2}gt^2 \leqslant x < L - \frac{1}{2}gt^2, \\ 1 & \text{for } L - \frac{1}{2}gt^2 < x, \end{cases} \tag{92}$$

where $L = 7.5$ m is the length of the tube. After the time

$$T = \sqrt{\frac{L}{g}} = 0.87 \text{ s} \tag{93}$$

we expect the phases to be fully separated and the liquid fraction will reach a stationary state. The other variables will slowly converge towards a stationary solution.

5.4.1. Results for the separation problem

For this problem, we used a constant timestep of $\Delta x/\Delta t = 2 \times 10^3$ m/s. The pressure and liquid volume fraction at the boundaries were determined by simple extrapolation.

In the following, the AUSMDV* and AUSMV* schemes are compared.Snapshots of the simulations at $T = 0.6$ s and $T = 1.0$ s are shown in Figs. 9 and 10. A grid of 100 cells was used. The reference solution was calculated using AUSMDV* on a grid of 1000 cells, except for Fig. 9 and volume fraction in Fig. 10, where the approximate analytical solutions given by (91) and (92) were used.

Fig. 9 shows the solution in the transient period where two volume fraction fronts, one upward and another downward directed, have been formed. In particular, we observe that both AUSMV* and AUSMDV* are able to handle the transition from two-phase to single-phase flow without loss of positivity. Comparison with the approximate analytical solution both in the liquid volume fraction and the liquid velocity variable clearly reveals that AUSMDV* is strongly superior to AUSMV* in the resolution of the discontinuous waves.

Fig. 10 shows the solution when the steady-state conditions have been reached, where the two-phase mixture is separated into a liquid part located at the bottom and a gas part located at the top. The plots clearly show the importance of the weak dissipative mechanism possessed by AUSMDV*: AUSMDV* is to a large extent able to reproduce the exact steady-state solution in the volume fraction variable, whereas AUSMV* performs much poorer on this fairly coarse grid.

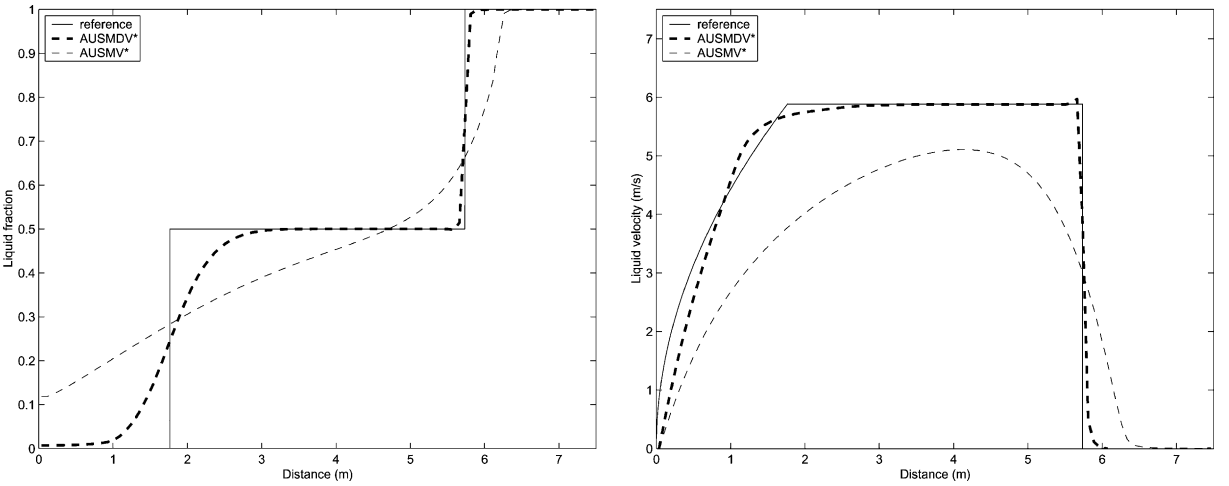

Fig. 9. Separation problem, snapshot at $T = 0.6$ s. Left: liquid fraction. Right: liquid velocity. The plots show the approximate solutions in the transient period on a grid of 100 cells.

For completeness, we have included the plots of the pressure and gas velocity as well. From the plot of the gas velocity, we observe that it becomes very large as the gas phase is disappearing. This is a result of our unphysical neglection of friction terms, which implies that no forces will balance the relatively strong hydrostatic pressure gradients induced by the heavy liquid phase.

5.4.2. Convergence

A further investigation of the accuracy of AUSMDV* on the volume fraction is made in Fig. 11, where the effect of grid refinement is illustrated. Although we have no stable Roe scheme to compare with, it seems that the effect of increased diffusion due to the transition fix is minimal. We also note that the AUSMDV* scheme gives good results compared to the upwind scheme of Cortes et al. [5] for this flow case.

5.5. Oscillating manometer problem

For our last numerical test, we consider the oscillating manometer problem introduced by Ransom [24]. This problem involves a moving liquid plug where the flow direction is time dependent. We hence believe that the numerical challenges presented by this problem are representative for typical transport pipeline simulations.

We consider a U-shaped tube of total length 20 m. The geometry of the tube is reflected in the x-component of the gravity field

$$g_x(x) = \begin{cases} g & \text{for } 0 \leqslant x \leqslant 5 \text{ m}, \\ g\cos\left(\frac{(x-5\text{ m})}{10\text{ m}}\pi\right) & \text{for } 5 \text{ m} < x \leqslant 15 \text{ m}, \\ -g & \text{for } 15 \text{ m} < x \leqslant 20 \text{ m}. \end{cases} \tag{94}$$

Initially, we assume that the liquid fraction is given by

$$\alpha_l(x) = \begin{cases} 10^{-6} & \text{for } 0 \leqslant x \leqslant 5 \text{ m}, \\ 0.999 & \text{for } 5 \text{ m} < x \leqslant 15 \text{ m}, \\ 10^{-6} & \text{for } 15 \text{ m} < x \leqslant 20 \text{ m}. \end{cases} \tag{95}$$

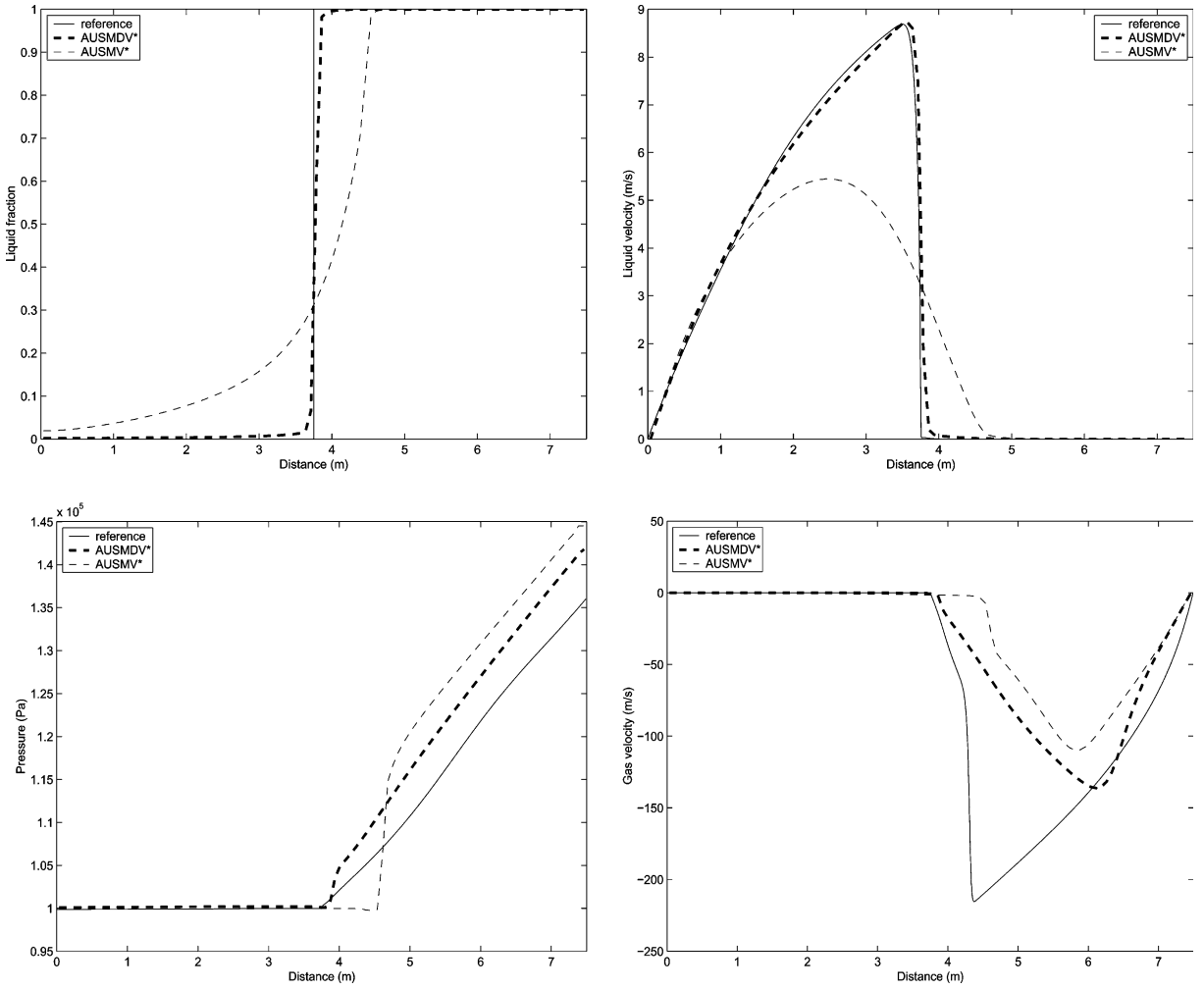

Fig. 10. Separation problem, snapshot at $T = 1.0$ s on a grid of 100 cells. Top left: liquid fraction. Top right: liquid velocity. Bottom left: pressure. Bottom right: gas velocity. At this time the phases are fully separated.

The initial pressure is assumed to be equal to the hydrostatic pressure distribution. The initial velocities of both phases are uniformly $v_k = V_0$, where $V_0 = 2.1$ m/s.

We treat the manometer as a closed loop, so that the left and right edges are connected to each other. Hence, there are no boundary conditions for this problem. We assume that the liquid column will move with uniform velocity under the influence of gravity, giving the following approximate analytical solution for the liquid velocity [23]

$$v_l(t) = V_0 \cos(\omega t), \tag{96}$$

where

$$\omega = \sqrt{\frac{2g}{L}} \tag{97}$$

and $L = 10$ m is the length of the liquid column.

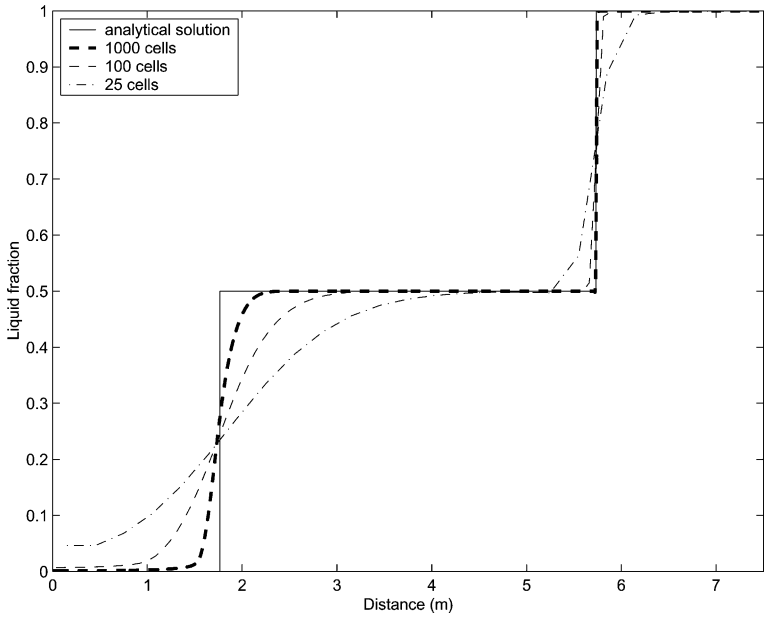

Fig. 11. Separation problem, $T = 0.6$ s. Liquid volume fraction. Grid refinement for the AUSMDV* scheme.

5.5.1. Numerical results

We used the AUSMDV* scheme on a grid of 100 cells with a timestep $\Delta x/\Delta t = 3000$ m/s. The time development of the liquid velocity is given in Fig. 12. The velocity is sampled at the lowest point (middle grid cell) of the manometer. We note that good accordance with the approximate analytical solution is obtained, although a small phase difference seems to develop. We also observe some numerical damping.

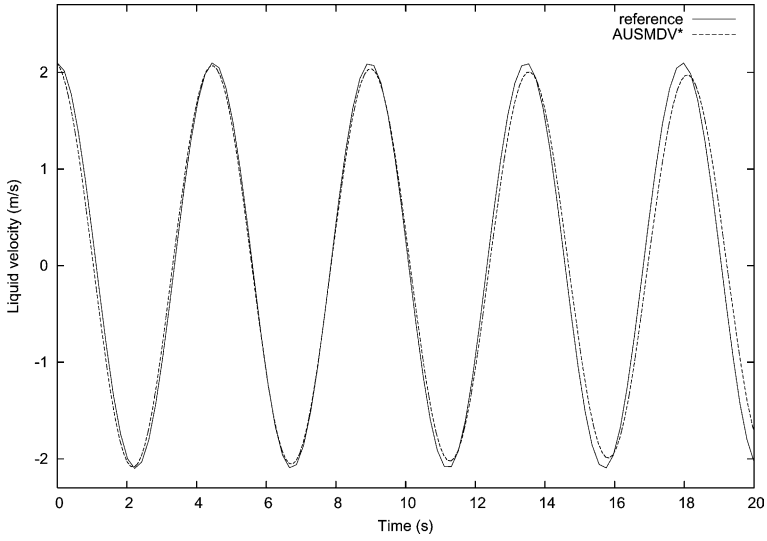

Fig. 12. Oscillating manometer, 100 cells. AUSMDV* scheme, time development of the mid-cell liquid velocity.

We remark that even though the scheme is flux-conservative, damping is expected as the gravity field is discretized using a simple Euler integration.

The distribution of the physical variables at the time $T = 20.0$ s is plotted in Fig. 13. There are no signs of any numerical oscillations. As expected, a hydrostatic pressure distribution is reproduced. There is very little dissipation in the volume fraction variable.

Remark 8. All the simulations we have considered have been first order accurate in space and time. In principle, second order accuracy may be achieved using Runge–Kutta time integration and MUSCL interpolation [15] of the primitive variables. This approach was successfully applied to similar flux-splitting schemes for the mixture model in [9]. The simulations in Sections 5.2–5.5 essentially demonstrate monotonicity of the numerical solutions, suggesting that for such cases similar strategies may be successful also for the current model.

However, the shock tube simulations in Section 5.1 show that more refined dissipation mechanisms must be developed before higher order techniques can be applied. In this respect, the good stability properties of the simpler FVS and van Leer schemes become of interest. As is demonstrated in for example [13], highly accurate solutions may be obtained by higher order techniques even if the basis schemes are diffusive. Of

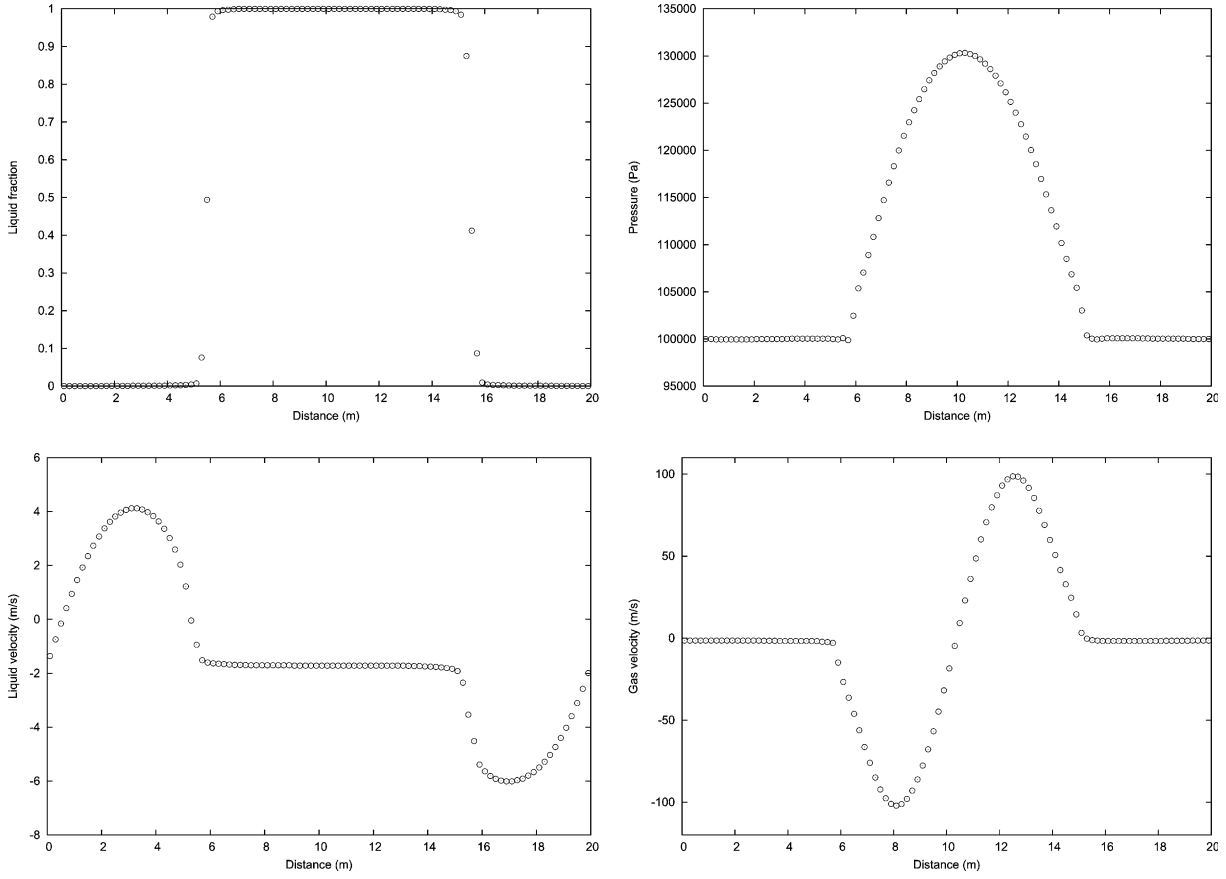

Fig. 13. Oscillating manometer, $T = 20.0$ s, 100 cells. AUSMDV* scheme. Top left: liquid fraction. Top right: pressure. Bottom left: liquid velocity. Bottom right: gas velocity.

particular interest here is the ability of FVS to handle the transition to one-phase flow without any kind of modification.

6. Summary

Schemes of FVS and van Leer type have been proposed for a two-phase flow model. Methods for removing numerical dissipation from these schemes have been explored. A mechanism for handling the difficult transition from two-phase to single-phase flow within this context has also been proposed. The resulting schemes, denoted as AUSMV* and AUSMD*, are demonstrated to have desirable properties. In particular, the AUSMV* is stable and the AUSMD* possesses an inherent accuracy comparable to an approximate Riemann solver, with a highly reduced computational cost. A hybrid AUSMDV* scheme, taking advantage of both these properties, has been proposed with particular focus on the kind of discontinuities expected to appear for slow transients associated with mass transport in pipelines. The proposed scheme does not provide the same level of robustness as an approximate Riemann solver for strong shocks. However, the framework has been demonstrated to contain the mechanism for providing accurate and efficient solutions to several benchmark two-phase flow problems.

Acknowledgements

The second author thanks the Norwegian Research Council for financial support through the "Petronics" programme. The authors also thank the referees for their valuable remarks which led to a substantial improvement of the first version of this paper.

References

[1] R. Abgrall, How to prevent pressure oscillations in multicomponent flow calculations, J. Comput. Phys. 125 (1996) 150–160.
[2] F. Barre et al., The cathare code strategy and assessment, Nucl. Eng. Des. 124 (1990) 257–284.
[3] K.H. Bendiksen, D. Malnes, R. Moe, S. Nuland, The dynamic two-fluid model OLGA: theory and application, SPE Prod. Eng. 6 (1991) 171–180.
[4] D. Bestion, The physical closure laws in the cathare code, Nucl. Eng. Des. 124 (1990) 229–245.
[5] F. Coquel, K. El Amine, E. Godlewski, B. Perthame, P. Rascle, A numerical method using upwind schemes for the resolution of two-phase flows, J. Comput. Phys. 136 (1997) 272–288.
[6] J. Cortes, A. Debussche, I. Toumi, A density perturbation method to study the eigenstructure of two-phase flow equation systems, J. Comput. Phys. 147 (1998) 463–484.
[7] J.R. Edwards, M.-S. Liou, Low-diffusion flux-splitting methods for flows at all speeds, AIAA J. 36 (1998) 1610–1617.
[8] J.R. Edwards, R.K. Franklin, M.-S. Liou, Low-diffusion flux-splitting methods for real fluid flows with phase transition, AIAA J. 38 (2000) 1624–1633.
[9] S. Evje, K.K. Fjelde, Hybrid flux-splitting schemes for a two-phase flow model, J. Comput. Phys. 175 (2002) 674–701.
[10] S. Evje, K.K. Fjelde, On a rough ausm scheme for a one-dimensional two-phase flow model, Comput. Fluids 32 (2003) 1497–1530.
[11] K.-K. Fjelde, K.H. Karlsen, High-resolution hybrid primitive-conservative upwind schemes for the drift flux model, Comput. Fluids 31 (2002) 335–367.
[12] A. Harten, P.D. Lax, B. Van Leer, On upstream differencing and Godunov schemes for hyperbolic conservation laws, SIAM Rev. 25 (1981) 35–61.
[13] G.-S. Jiang, D. Levy, C.-T. Lin, S. Osher, E. Tadmor, High-resolution nonoscillatory central schemes with nonstaggered grids for hyperbolic conservation laws, SIAM J. Numer. Anal. 25 (1998) 2147–2168.
[14] M. Larsen, E. Hustvedt, P. Hedne, T. Straume, Petra: A novel computer code for simulation of slug flow, in: SPE Annual Technical Conference and Exhibition, SPE 38841, October 1997, pp. 1–12.
[15] B.V. Leer, Towards the ultimate conservative difference scheme V. A second-order sequel to Godunov's method, J. Comput. Phys. 32 (1979) 101–136.

[16] R.J. LeVeque, Numerical Methods for Conservation Laws, second ed., Birkhäuser Verlag, 1992, pp. 89–93.
[17] M.-S. Liou, A sequel to AUSM: AUSM(+), J. Comput. Phys. 129 (1996) 364–382.
[18] M.-S. Liou, C.J. Steffen, A new flux splitting scheme, J. Comput. Phys. 107 (1993) 23–39.
[19] J.M. Masella, I. Faille, T. Gallouet, On an approximate Godunov scheme, Int. J. Comput. Fluid. Dyn. 12 (1999) 133–149.
[20] Y.Y. Niu, Simple conservative flux splitting for multi-component flow calculations, Numer. Heat Trans. 38 (2000) 203–222.
[21] Y.-Y. Niu, Advection upwinding splitting method to solve a compressible two-fluid model, Int. J. Numer. Meth. Fluids 36 (2001) 351–371.
[22] S. Osher, Riemann solvers, the entropy conditions, and difference approximations, SIAM J. Numer. Anal. 21 (1984) 217–235.
[23] H. Paillère, C. Corre, J.R.G Cascales, On the extension of the AUSM+ scheme to compressible two-fluid models, Comput. Fluids 32 (2003) 891–916.
[24] V.H. Ransom, Numerical bencmark tests, Multiphase Sci. Tech. 3 (1987) 465–473.
[25] P.L. Roe, The use of Riemann problem in finite difference schemes, Lect. Notes Phys. 141 (1980) 354–359.
[26] P.L. Roe, Approximate Riemann solvers, parameter vectors, and difference schemes, J. Comput. Phys. 43 (1981) 357–372.
[27] J.E. Romate, An approximate Riemann solver for a two-phase flow model with numerically given slip relation, Comput. Fluids 27 (1998) 455–477.
[28] R. Saurel, R. Abgrall, A multiphase godunov method for compressible multifluid and multiphase flows, J. Comput. Phys. 150 (1999) 425–467.
[29] H.B. Stewart, Stability of two-phase flow calculation using two-fluid models, J. Comput. Phys. 33 (1979) 259–270.
[30] H.B. Stewart, B. Wendroff, Review article; two-phase flow: models and methods, J. Comput. Phys. 56 (1984) 363–409.
[31] I. Tiselj, S. Petelin, Modelling of two-phase flow with second-order accurate scheme, J. Comput. Phys. 136 (1997) 503–521.
[32] I. Toumi, An upwind numerical method for two-fluid two-phase flow models, Nucl. Sci. Eng. 123 (1996) 147–168.
[33] I. Toumi, A. Kumbaro, An approximate linearized Riemann solver for a two-fluid model, J. Comput. Phys. 124 (1996) 286–300.
[34] J.A. Trapp, R.A. Riemke, A nearly-implicit hydrodynamic numerical scheme for two-phase flows, J. Comput. Phys. 66 (1986) 62–82.
[35] Y. Wada, M.-S. Liou, An accurate and robust flux splitting scheme for shock and contact discontinuities, SIAM J. Sci. Comput. 18 (1997) 633–657.